A PRACTICAL GRID GENERATION PROCEDURE FOR THE DESIGN OF FREE-FORM STRUCTURES

Boqing Gao[1], Tierui Li[1], Teng Ma[2], Jun Ye[1,3], Jurgen Becque[3] and Iman Hajirasouliha[3]

1 College of Civil Engineering and Architecture, Zhejiang University, Hangzhou, China

2 China United Engineering Corporation, Hangzhou, China

3 Department of Civil and Structural Engineering, The University of Sheffield, Sheffield, UK

Corresponding author: zjuyejun@gmail.com

Abstract

Computer aided design software enables the rapid conceptual creation of a curved surface geometry, whereas it is neither a convenient nor an obvious task for engineers to create a discrete grid structure on a complex surface that meets architectural and aesthetic requirements. This emphasizes the importance of grid generating tools and methods in the initial design stage. This paper presents an efficient design tool for the synthesis of free-form grid structures based on the "guide line" method, employing a fast and straightforward approach which achieves grids with rods of balanced length and fluent lines. The process starts with defining a limited number of curves (named the "guide lines") on the surface, which are then used to determine the directions of the 'rods' of the grid. Two variations of this concept are introduced in this paper: the 'Guide Line Scaling Method' (GSM) and the 'Two Guide Lines with Two End Vertices Method' (2G2VM). Case studies are provided which illustrate the successful execution of these procedures. The results show that the free-form grid structures generated with the proposed methods feature a regular shape and fluent lines, thereby satisfying aesthetic requirements. These two methods have been programmed into the software ZD-Mesher, enabling rapid grid generation for structural design purposes.

Keywords: Free-form surface; Grid structure; Guide line; Free form structures; Guide line scaling method.

1 Introduction

New techniques in computer aided design, such as parametric modelling and scripting, have enabled a new level of sophistication in design. Among other developments, this has facilitated the increased inclusion of 3D free-form surfaces in structures, marrying the expression of architectural creativity with the application of cutting-edge technology. Complex free-form structures are one of the most visually striking trends in contemporary architecture. A number of structures with attractive designs and eye-catching shapes have recently been erected, as shown in Fig. 1 (a) to (d). While they are constructed with sometimes vastly different materials, they all exemplify the emergence of free-form grid structures.

(a) British Museum Great Court (London, UK)

(b) Vela-roof in Milan Trade Fair (Milan, Italy)[1]

(c) Shenzhen Sports Center stadium (Shenzhen, China) (d) Toledo timber grid shell (Naples, Italy)[2]

Fig. 1. Examples of free-form grid structures.

If a curved surface with a suitable form is chosen and well-positioned supports are added, an efficient flow of the forces within the structure can be obtained [3], where a single layer grid-shell

structure consisting of a lattice of rods can be used to transmit the external loads down to the foundations mainly by means of axial forces within the members. This structural form often brings benefits in the form of reductions in material usage, enhanced aesthetics, better structural performance, ease of fabrication and an increase in unobstructed service space. However, it is not always obvious how to create an efficient grid structure on a given surface. For example, Fig.2 illustrates the roof structure of Daishan Sports Stadium in China by Ding and Wang [4]. The curved free-form surface shown in Fig.2 (a) was determined by the architect in the early conceptual design stage, but subsequently the structural analysis required an arrangement of nodes and elements on the curved surface. In this particular case, this was achieved manually with tedious iteration, with the result being shown in Fig.2 (b). Fig.2 (c) shows the resulting structure in an architectural rendering with the skeleton in Fig.2 (b) covered by roof panels. Given the increasing popularity of free-form grid structures, a practical grid generation tool which can quickly and efficiently generate a structural grid on a given free-form surface is necessary in order to assist structural designers, particularly in the early design stage.

Earlier studies on free-form grid structures have mainly concentrated on the structural design aspects [1, 5], form-finding methodologies [2, 6], connections [7] and optimization techniques [8-10]. However, previous research on grid generating methodologies is rather limited. Park et al. [11] and Shepherd and Pearson [12] demonstrated that topology optimization methods can be used to create an efficient structural grid on a predefined surface, with both studies presenting a layout optimization algorithm for both single and double layer shells in the conceptual design stage. Wu et al. [13] conducted theoretical and experimental research on grid generation for a cable supported dome using topology optimization techniques. However, a drawback of all these topology optimization studies [11-13] is that the resulting topology is rather coarse and cannot directly be used in design (i.e. some refinement is required).

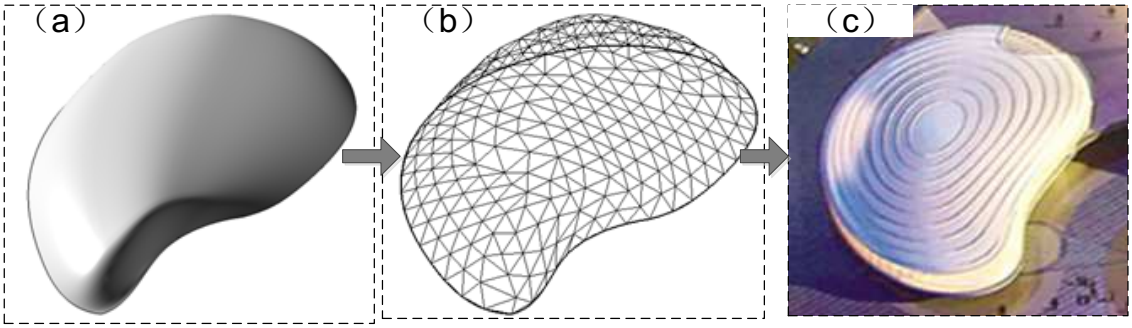

Fig. 2. Creation of a free-form single layer grid structure (Daishan Sports Stadium, Daishan City, China) [4].

Research has also been conducted at the University of Cambridge [14] with the aim of generating practical and efficient grids over free-form surfaces, while considering the mechanical performance under multiple load cases. In this process a discrete grid structure consisting of repeating quadrilateral or triangular cells was first specified. A homogenization process was then used to represent this lattice of rods by anisotropic continuum shell elements for the purpose of structural analysis. The rod orientations were then optimized using a Genetic Algorithm.

In other research by Su et al. [15], the main stress trajectories on the surface under loading were used in a grid generation tool. A modified 'advancing front' mesh technique was thereby used. While this method is geared towards an efficient structural performance of the grid, an iterative process and FE analysis are needed in the grid generation procedure, requiring significant computational time. Another drawback of this method is that it may lead to a non-uniform grid with distorted unit cells, as show in the generated grid for Sun Valleys at the Shanghai EXPO in Fig.3.

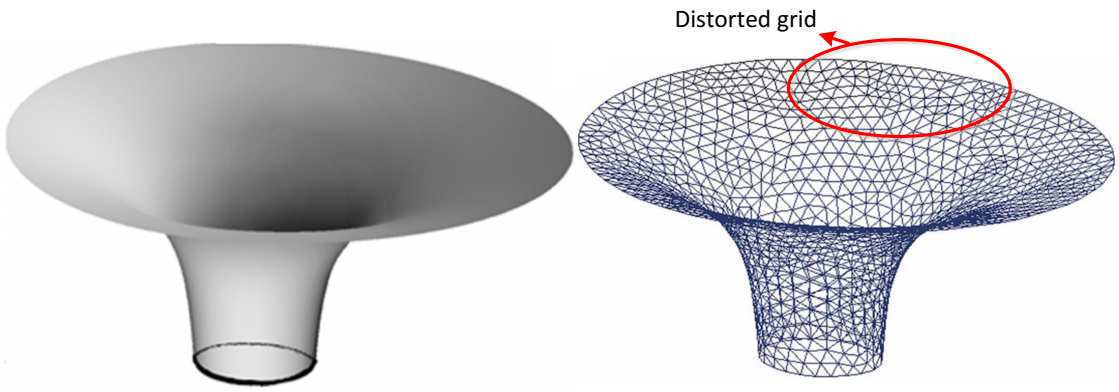

Fig. 3. Grid layout results generated in [15].

In practice, rather than optimizing structural performance, it is sometimes more important to generate a grid on a curved surface which is aesthetically pleasing and which satisfies the uniformity criteria, i.e. where unit cells have regular shapes and rods are composed of fluent lines. Therefore, many of the previous research studies have concentrated on mesh generation over a surface without taking into account structural performance. For example, Shepherd and Richens [3] proposed the Subdivision Surface method, where an initial triangular or quadrilateral mesh is first imposed onto a free-form surface and then subdivided over a number of iterations to fit the original surface. An alternative approach was applied in the design of the Vela-roof of the Milan Trade Fair [1], where the rod directions and connection positions were generated using clusters of auxiliary lines. In a first stage, auxiliary lines were introduced to generate grid cells in the nearly non-curved regions. In the next step, additional lines aligned with the principal flow of stresses were added to the curved regions using a different shape of grid. Iterative adjustments were then made in order to optimize the grid. Liu et al.[16] proposed an approach to automatically generate a 2D quadrilateral mesh under arbitrary line constraints. The method begins with discretizing the constraining lines within the domain into a number of segments. Next, a triangular mesh is generated using the Delaunay Triangulation Algorithm, taking into account the initial discretized lines. The triangular mesh is then transformed into an all-quad mesh using an advancing front method, starting from the line constraints, which roughly keeps the features of the initial triangular mesh. Finally, the resulting quadrilateral mesh is optimized to reduce the number of irregular nodes. Du Peloux et al [17] and Hennicke and Schaur [18] used a “compass method” to generate a quadrilateral mesh with constant rod length on a NURBS surface. In this method two initial crossing guide-curves are drawn on the surface and divided by a compass into segments of constant chord length. The nodes are then used as the centres of circles, drawn by the compass on the surface, and the intersecting points of the circles form new nodes in a repeating process. Based on the

Delaunay triangulation method, Muylle et al. [19] developed a mesh generation procedure intended for finite element analysis by presenting a new point creation scheme for obtaining unstructured uniformly sized two-dimensional triangular meshes. It is shown in their paper that the final mesh depends significantly on the initial distribution of points. In another research study by Branets and Garey [20], a local cell quality metric which takes into account the element shape and size was proposed and used to construct a variational functional for a grid smoothing algorithm. The method used the geometric quality metric as the objective and applied a damped Newton scheme to solve the optimization problem in order to obtain a grid with better quality.

Grid generation methods, if implemented in software, can provide an interactive design environment which does not suppress creativity, but rather makes it possible to receive instant feedback on an initial design. Such software also allows the exploration of different design options and can incorporate multi-objective optimization algorithms to help the user to quickly identify a particularly promising design direction [3].

This paper aims to develop a practical methodology to quickly generate a grid on a predefined curved surface with given boundaries. The method focusses on obtaining a regular geometry, rather than on structural performance. It allows grid generation based on a limited number of guidelines using operations such as offset, scaling, rotation and projection. While structural performance is currently not taken into account in the proposed methodology, a performance aspect can be added by selecting guidelines based on the stress trajectories under governing loads [21]. Optionally, a further sizing optimization of the structural members can then be performed based on the generated grids. The here proposed methodology is innovative on the basis of introducing the concept of a “guideline” and two new ways of grid generation are presented, namely the ‘guide line scaling’ method (GSM) and the ‘two guide lines with two end vertices’ method (2G2VM). The proposed algorithms have been implemented in the general-purpose

programming language C++ and a Graphical User Interface has been developed. A number of case studies are presented to illustrate the successful execution of the algorithms and the effectiveness of the software.

2 Guide Line Definition

To be practically relevant, the generated grid should meet certain aesthetic and architectural requirements. For a given surface there are various solutions which may satisfy those requirements, even when expressed in terms of objective criteria such as grid regularity, rod uniformity, and pattern fluency. A simple example is shown in Fig.4 (a) and Fig.4 (b), where two grid patterns are considered: an orthogonal grid parallel to the sides and an orthogonal-diagonal grid. Which one is the more favourable pattern in terms of appearance most likely depends on the individual preference of the architect, although one could argue that the grid style presented in Fig.4 (b) portrays a sense of vividness and is therefore preferable.

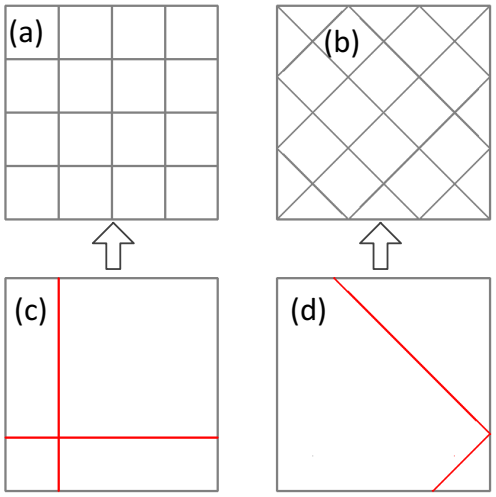

Fig. 4. Guide lines and generated grid on a plane surface: (a) Regular grid parallel to the edges; (b) Diagonal grid at 45°; (c), (d) corresponding guide lines.

Given this context, a practical and feasible approach consists of defining a ‘guide line’ on the surface that sets the tone of the grid and reveals the intent of the designer. The red curves shown

in Fig.4 (c) and Fig.4 (d) fulfill exactly this function in this simplified example. The selection of guide line depends on the designer's preference. An innovative architect might choose a guide line that will provide less obvious solutions than the grids shown in Fig.4. This will however not hinder the application of the proposed method. Rather the efficiency of the algorithm will assist the designer in assessing multiple options in an acceptable time.

3 Surface Representation

In the proposed approach, the Non-Uniform Rational B-Spline (NURBS) is applied to describe curves and surfaces. To this end, the B-spline basis functions need to be introduced first. Let $\mathbf{U}=\{u_0,...,u_n\}$ be a non-decreasing sequence of rational numbers, i.e., $u_i \le u_{i+1}$, $i=0,...,n-1$. The numbers u_i are called the 'knots', and **U** is the 'knot vector'. The i^{th} B-spline basis function of degree p, denoted by $N_{i,p}(u)$, is then defined in terms of an independent variable u as follows [22]:

$$N_{i,0}(u)=\begin{cases}1 & \text{if } u_i \le u < u_{i+1}\\ 0 & \text{otherwise}\end{cases}$$
$$N_{i,p}(u)=\frac{u-u_i}{u_{i+p}-u_i}N_{i,p-1}(u) \quad \frac{u_{i+p+1}-u}{u_{i+p+1}-u_{i+1}}N_{i+1,p-1}(u) \tag{1}$$

In the above equations, i = 0,…, n-p-1, so that there are n-p basis functions of degree p. Note that $N_{i,0}(u)$ is a step function which is identically equal to zero everywhere, except in the half-open interval $u \in [u_i, u_{i+1})$. The higher order basis functions $N_{i,p}(u)$ are then formed by taking a linear combination of two basis functions of degree (p-1). The half-open interval $[u_i, u_{i+1})$ is commonly called the i^{th} knot span. It can have zero length since knots do not need to be distinct.

A p^{th}-degree NURBS curve is shown in Fig. 5 and is defined by [22]:

$$\mathbf{C}(u)=\big(x(u), y(u), z(u)\big) \quad \frac{\sum_{i=0}^{n} N_{i,p}(u)w_i\mathbf{P}_i}{\sum_{i=0}^{n} N_{i,p}(u)w_i} \quad a \quad u \quad b \tag{2}$$

where $\mathbf{P}_i = (x_i, y_i, z_i)$ are the control points, w_i are the weight factors, n is the number of control points and $N_{i,p}(u)$ are the p^{th}-degree B-spline basis functions according to Eq. (1), defined on the knot vector:

$$U = \{\underbrace{a,...,a}_{p+1}, u_{p+1},...,u_{r-p-1}, \underbrace{b,...,b}_{p+1}\} \tag{3}$$

where $r = n + p + 1$ is the number of knots. Adding the zero length knot spans in Eq. (3) ensures that there are exactly n + 1 basis functions of degree *p*. It is also noted that the weight factors w_i are constrained to positive values for all i.

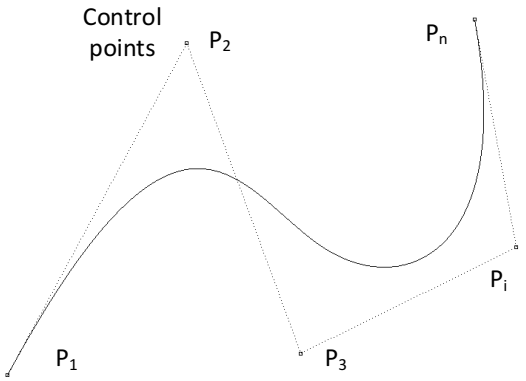

Fig. 5. The relationship between the curve and its control points.

Introducing the notation:

$$R_{i,p}(u) = \frac{N_{i,p}(u) w_i}{\sum_{j=0}^{n} N_{j,p}(u) w_j} \tag{4}$$

Eq. (2) can be rewritten in the form:

$$\mathbf{C}(u) = \sum_{i=0}^{n} R_{i,p}(u) \cdot \mathbf{P}_i \tag{5}$$

where $\{R_{i,p}(u)\}$ are the rational basis functions, which are piecewise rational functions of $u \in [a,b]$.

In general, NURBS defined curves have the following two important geometric characteristics [22, 23], which will prove useful at a later stage:

(1) $\sum_{i=0}^{n} R_{i,p}(u) = 1$ for all $u \in [a,b]$, which, together with $R_{0,p}(a) = R_{n,p}(b) = 1$, implies: $\mathbf{C}(a) = \mathbf{P}_0$ and $\mathbf{C}(b) = \mathbf{P}_n$. In other words, the starting point of the curve is the first control point, while the end point of the curve is the last control point, as shown in Fig. 5.

(2) Affine invariance: an affine transformation can be applied to the curve by applying it to the control points. Affine transformations include translations, rotations, scaling and shearing. NURBS curves are also invariant under perspective projections.

An NURBS surface (shown in Fig. 6) of degree *p* in the *u* direction and degree *q* in the *v* direction is a bivariate vector-valued piecewise rational function of the form [22]:

$$\mathbf{S}(u,v) = \frac{\sum_{i=0}^{n}\sum_{j=0}^{m} N_{i,p}(u) N_{j,q}(v) w_{i,j} \mathbf{P}_{i,j}}{\sum_{i=0}^{n}\sum_{j=0}^{m} N_{i,p}(u) N_{j,q}(v) w_{i,j}} \quad a \le u \le b, c \le v \le d \tag{6}$$

where $\mathbf{P}_{i,j}$ forms a bidirectional control net of points, $w_{i,j}$ are the weight factors and $N_{i,p}(u)$ and $N_{j,q}(v)$ are the non-uniform rational B-spline basis functions defined on the knot vectors:

$$\begin{cases} U = \{\underbrace{a,\ldots,a}_{p+1}, u_{p+1},\ldots,u_{r-p-1}, \underbrace{b,\ldots,b}_{p+1}\} \\ V = \{\underbrace{c,\ldots,c}_{q+1}, v_{q+1},\ldots,v_{s-q-1}, \underbrace{d,\ldots,d}_{q+1}\} \end{cases} \tag{7}$$

where $r = n + p + 1$ and $s = m + q + 1$.

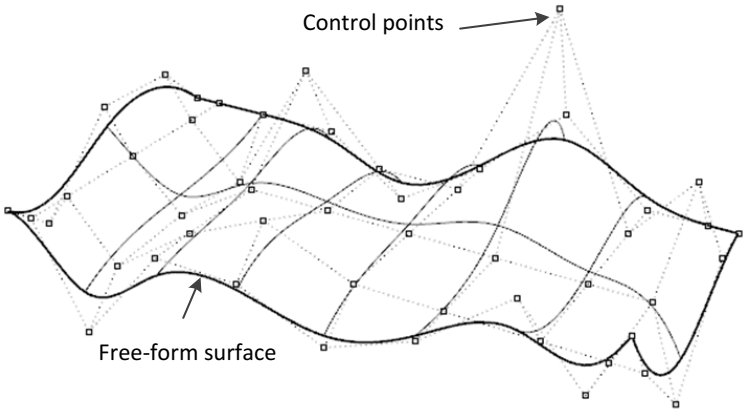

Fig. 6. Curved surface and its control points.

The above NURBS equations for describing surfaces and curves can be used to represent a curved architectural surface, as well as a guideline for grid generation (as introduced in the previous section of the paper). A guideline lying on the NURBS surface $(x_{u,v}, y_{u,v}, z_{u,v}) = \mathbf{S}_{x,y,z}(u,v)$ is thus defined by an NURBS curve in three-dimensional space as:

$$(x_w, y_w, z_w) = \mathbf{C}_{x,y,z}(w) \tag{8}$$

It is thereby noted that the guideline also has a 2D representation in the parameter space (u,v) of the surface. This is illustrated in Fig. 7. Indeed, the 3D guideline can be seen as the result of a two-time mapping procedure, with a two-dimensional NURBS curve $(u_w, v_w) = \mathbf{C}_{u,v}(w)$ lying in the parametric field of the surface (Fig. 7) as the intermediate step:

$$(x_w, y_w, z_w) = \mathbf{S}_{x,y,z}(u_w, v_w) \quad \mathbf{S}_{x,y,z}(\mathbf{C}_{u,v}(w)) \tag{9}$$

It is obvious that all of the coordinates obtained by this two-time mapping method lie exactly on the surface so that the guide line is embedded within the curved surface. One of the advantages of having this 2D representation of the guideline (and any subsequent curves generated on the surface) in the parameter space (u,v) is that points of intersection between curves are much easier calculated in the space (u,v) and then mapped onto the surface than calculated in 3D space.

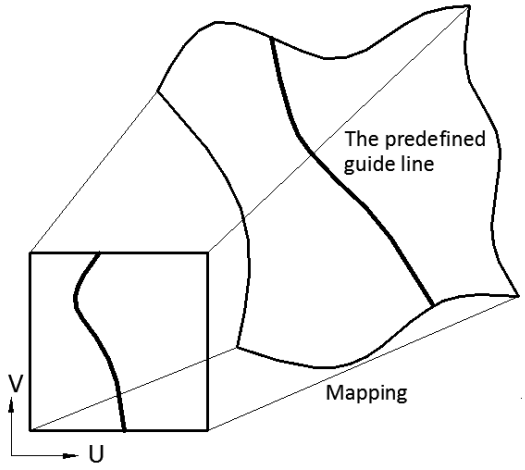

Fig. 7. Mapping method from parametric space to 3D space.

A three-dimensional curve can easily be obtained from its two-dimensional representation by the above mapping procedure. The solution to the inverse problem (obtaining the 2D representation when the curve is known in 3D space) is documented in [22].

4 Projecting a Point onto a Surface

An algorithm to project a generic point $\mathbf{P} = (x,y,z)$ perpendicularly onto a surface $\mathbf{S}(u,v)$ is needed in both grid-generating methods.

In order to achieve this, the following vector field is first defined:

$$\mathbf{r}(u,v) = \mathbf{S}(u,v) - \mathbf{P} \tag{10}$$

which is made subject to the following two conditions:

$$\begin{cases} \mathbf{f}(u,v) = \mathbf{r}(u,v) \cdot \mathbf{S}_u(u,v) = 0 \\ \mathbf{g}(u,v) = \mathbf{r}(u,v) \cdot \mathbf{S}_v(u,v) = 0 \end{cases} \tag{11}$$

The subscripts u and v thereby indicate differentiation with respect to u and v, respectively. The above equations express that a point on the surface $\mathbf{S}(u,v)$ needs to be found at which the normal to the surface points to the point $\mathbf{P} = (x,y,z)$. The above equations can be solved iteratively by defining the following matrices in the i^{th} iteration:

$$\boldsymbol{\delta}_i = \begin{bmatrix} \Delta u \\ \Delta v \end{bmatrix} = \begin{bmatrix} u_{i+1} - u_i \\ v_{i+1} - v_i \end{bmatrix} \tag{12}$$

$$\mathbf{J}_i = \begin{bmatrix} \mathbf{f}_u & \mathbf{f}_v \\ \mathbf{g}_u & \mathbf{g}_v \end{bmatrix} = \begin{bmatrix} |\mathbf{S}_u|^2 + \mathbf{r} \cdot \mathbf{S}_{uu} & \mathbf{S}_u \cdot \mathbf{S}_v + \mathbf{r} \cdot \mathbf{S}_{uv} \\ \mathbf{S}_u \cdot \mathbf{S}_v + \mathbf{r} \cdot \mathbf{S}_{vu} & |\mathbf{S}_v|^2 + \mathbf{r} \cdot \mathbf{S}_{vv} \end{bmatrix} \tag{13}$$

$$\boldsymbol{\kappa}_i = -\begin{bmatrix} \mathbf{f}(u_i, v_i) \\ \mathbf{g}(u_i, v_i) \end{bmatrix} \tag{14}$$

All the functions in the matrix $\mathbf{J}_i$ are thereby evaluated at the point (u_i, v_i). In the i^{th} iteration, the 2×2 system of linear equations in the unknown vector $\boldsymbol{\delta}_i$ is solved:

$$\mathbf{J}_i\boldsymbol{\delta}_i = \boldsymbol{\kappa}_i \tag{15}$$

After obtaining $\boldsymbol{\delta}_i$ the new coordinates (u, v) are calculated:

$$u_{i+1} = u_i + \Delta u, \quad v_{i+1} = v_i + \Delta v \tag{16}$$

The convergence criteria are given by:

$$\left|\boldsymbol{\delta}_i\right| \le \varepsilon_1 \tag{17}$$

$$\frac{\left|\mathbf{S}_u(u_i,v_i)\cdot(\mathbf{S}(u_i,v_i)-\mathbf{P})\right|}{\left|\mathbf{S}_u(u_i,v_i)\right|\left|\mathbf{S}(u_i,v_i)-\mathbf{P}\right|} \le \varepsilon_2, \quad \frac{\left|\mathbf{S}_v(u_i,v_i)\cdot(\mathbf{S}(u_i,v_i)-\mathbf{P})\right|}{\left|\mathbf{S}_v(u_i,v_i)\right|\left|\mathbf{S}(u_i,v_i)-\mathbf{P}\right|} \le \varepsilon_2 \tag{18}$$

where ε_1 is the tolerance for the Euclidean distance between successive iteration points, while ε_2 is the tolerance for orthogonality of the vector **r** relative to the tangent plane to the surface. The value of ε_2 was taken as 10^{-6} in the examples presented in this paper, while the values of ε_1 ranged from 10^{-3} mm to 1 mm, depending on the magnitude of the dimensions of the surface. At the same time, it should be checked in each iteration whether the points (u_i, v_i) remain within the boundaries of the surface $\mathbf{S}(u,v)$.

In the next Sections 5 and 6, the “Guideline Scaling Method” (GSM) and the “Two Guide Lines with Two End Vertices Method” (2G2VM) will be introduced. These methods will be used to generate grids on a number of surfaces and a comparison will be carried out with the results of a “Mapping Method” presented in [24], which was developed for mesh generation in finite element analysis. This latter method also works on the principle explained in Fig.7.

In Section 7 the steel-and-glass grid of the British Museum Great Court Roof will be investigated as a benchmark example for the various algorithms. The results of the GSM and the 2G2VM will be compared with the grid originally presented by Williams [25], who analytically defined the shape of the roof in the form of mathematical functions.

5 Guide Line Scaling Method (GSM)

5.1 Description of Algorithm

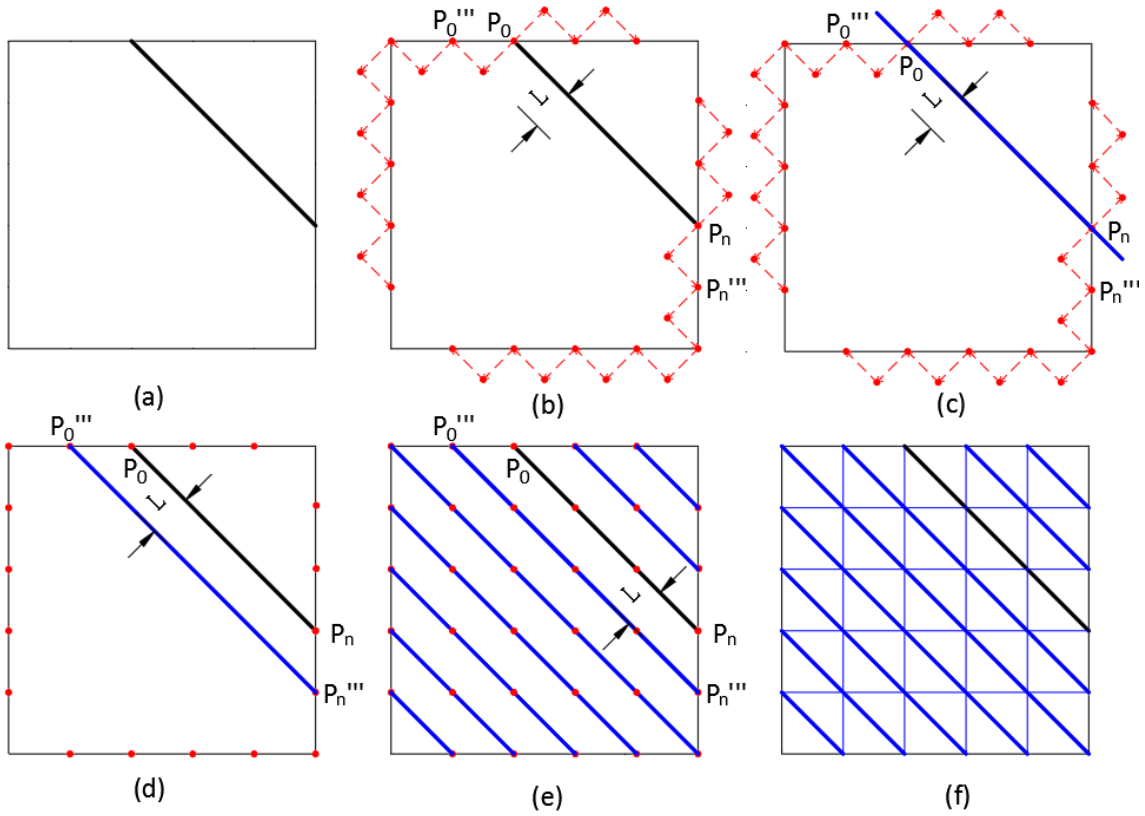

Fig. 8. Main steps of GSM, as schematically illustrated for a flat surface: (a) definition of initial guide line; (b) generation of new end points; (c) scaling of the guideline; (d) translation/rotation of the guideline, followed by projection onto the surface; (e) generation of grid points; (f) final triangular grid.

In the GSM, the following steps are taken (Fig. 8):

1. An initial guide line is sketched on the curved surface. Alternatively, one of the boundaries of the surface, if appropriate, may be selected as a guide line (Fig.8 (a)).
2. An NURBS representation $\mathbf{S}(u,v)$ is fitted to the surface, while the initial guide line defined on the surface in Step 1 is represented by an NURBS curve $\mathbf{C}_0$ in three-dimensional space. The control points of the NURBS curve $\mathbf{C}_0$ are $\mathbf{P}_i$, $i=0,1,\ldots,n$. $\mathbf{P}_0$ and $\mathbf{P}_n$ are the first and the last

control points, which are also the two end points of the curve (as explained in Section 3) (Fig.8 (b)).

3. In order to generate a new curve on the surface in the shape of the original guide line, the end points of the original guide line $\mathbf{P}_0$ and $\mathbf{P}_n$ are first moved forward in space by a constant (chosen) distance L in the direction of the vector

$$\vec{D} = \pm \vec{N} \times \vec{\tau} \tag{19}$$

As shown in Fig. 9, $\vec{N}$ is the normal vector to the surface at the end point of the guide line and $\vec{\tau}$ is the tangent vector to the guide line. Therefore, $\vec{D}$ constitutes a direction perpendicular to the guide line in the tangent plane of the surface.

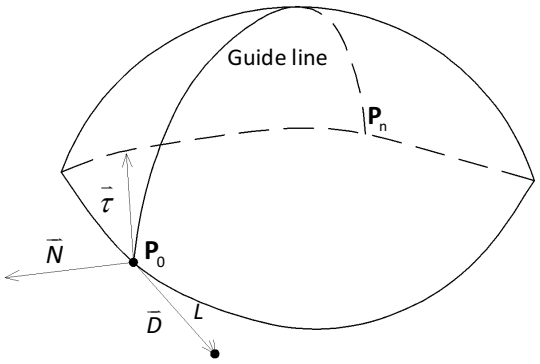

Fig. 9. Advancing direction of the guide line.

It is clear that, in general, the end point of the vector $\vec{D}$ does not lie on the surface boundary. Therefore, the end point of $\vec{D}$ is first projected onto the surface, using the procedure explained in Section 4 of the paper. This yields a point D' on the surface, as well as the normal $\vec{N}_2$ to the surface at D' (Fig. 10). A straight line through the point D' is then defined with direction:

$$\vec{T} = \vec{D} \times \vec{N}_2 \tag{20}$$

The point on the boundary curve with the shortest distance to this straight line is then determined using the procedure documented in [26]. Carrying out this procedure for both end

points $\mathbf{P}_0$ and $\mathbf{P}_n$ of the original guide line results in two new points $\mathbf{P}_0'''$ and $\mathbf{P}_n'''$ on the boundary curve.

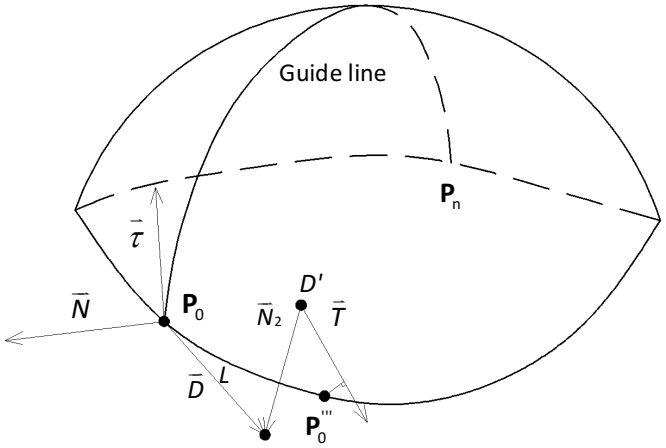

Fig.10. Obtaining the next end point on the boundary curve.

4. $\mathbf{P}_0'''$ and $\mathbf{P}_n'''$ are then connected with a new curve in the shape of the original guideline. An affine transformation of the original guideline which, in the general case, consists of a scaling, a translation, and a rotation, is thereby necessary (Fig.8 (c)).

Let l_1 be the Euclidean distance between $\mathbf{P}_0$ and $\mathbf{P}_n$, while the Euclidean distance between $\mathbf{P}_0'''$ and $\mathbf{P}_n'''$ is denoted by l_2. If $l_1 \neq l_2$, a scaling of the original guide line is required:

$$\mathbf{P}_i' = (\mathbf{P}_i - \mathbf{P}_n) \times l_2 \div l_1 + \mathbf{P}_n,\ i = 0,1,...,n \tag{21}$$

where $\mathbf{P}_i'$ are the control points of the scaled curve.

The control points are then translated according to the formula below:

$$\mathbf{P}_i'' = \mathbf{P}_i' + (\mathbf{P}_n''' - \mathbf{P}_n),\ i = 0,1,...,n \tag{22}$$

where $\mathbf{P}_i''$ are the control points after the curve is scaled and translated.

If $\mathbf{P}_0''$ and $\mathbf{P}_0'''$ happen to coincide with each other, then the translated control points are the end points of the new curve. In general, however, $\mathbf{P}_0''$ and $\mathbf{P}_0'''$ do not coincide and the scaled and translated guideline also needs to be rotated so that $\mathbf{P}_0''$ and $\mathbf{P}_0'''$ coincide (Fig. 11).

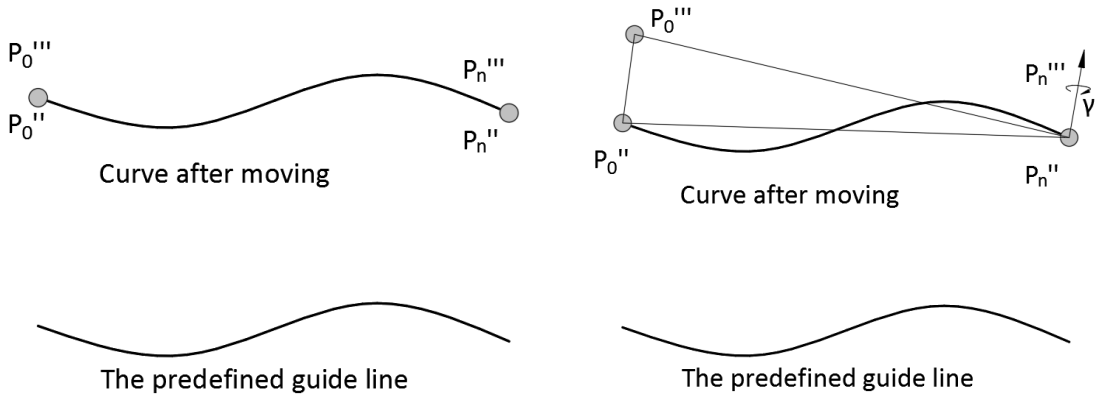

(a) $\mathbf{P}_0''$ and $\mathbf{P}_0'''$ are coinciding (b) $\mathbf{P}_0''$ and $\mathbf{P}_0'''$ are not coinciding.

Fig. 11. Adjustment of the generated curves.

The axis of rotation is the straight line through the point $\mathbf{P}_n''$ (= $\mathbf{P}_n'''$) with direction $\mathbf{R}$, perpendicular to the plane determined by the three points: $\mathbf{P}_0'''$, $\mathbf{P}_0''$ and $\mathbf{P}_n''$:

$$\mathbf{R} = (\mathbf{P}_0'' - \mathbf{P}_n'') \times (\mathbf{P}_0''' - \mathbf{P}_n'') \tag{23}$$

The angle of rotation γ is determined by:

$$\gamma = 2\arcsin\frac{\left|\mathbf{P}_0''' - \mathbf{P}_0''\right|}{2\left|\mathbf{P}_0'' - \mathbf{P}_n''\right|} \tag{24}$$

The coordinates of the new control points $\mathbf{P}_i'''$ can then be obtained from the coordinates of $\mathbf{P}_i''$ through a coordinate transformation. A new curve $\mathbf{C}_1$ is subsequently defined by the control points $\mathbf{P}_i'''$ and the same weight factors, knot vector and degree as the original guide line. However, this curve $\mathbf{C}_1$, in the general case, does not lie on the curved surface $\mathbf{S}(u,v)$.

5. A number of discrete points on the curve $\mathbf{C}_1$ are projected onto the surface $\mathbf{S}(u,v)$, using the procedure explained in Section 4 of this paper.
6. After these points on the surface $\mathbf{S}(u,v)$ are obtained, the corresponding points (u,v) in the parameter space are calculated. A 2D NURBS curve is then fitted through these points in the

parameter space and mapped back onto the 3D surface. This is done to ensure that the new curve is completely embedded within the surface $\mathbf{S}(u,v)$ (Fig.8 (d)).

7. The above procedure is then repeated a sufficient number of times by advancing successive curves to cover the whole surface (Fig.8 (e)). These curves are then subdivided along their lengths into an integer number of segments with equal chord length, approximately equal to the preferred rod length L_1 of the grid (Fig.8 (e)), with the aim of achieving regular grid cells. The following algorithm is used:

   Starting from one end of the curve, segments with a chord length L_1 are added along the curve until the other end is reached. A 'left-over' segment with chord length L_2 is typically encountered at the other end (Fig. 12). If L_2 is sufficiently small (e.g. less than $\delta = 0.2L_1$), the final segment with length L_2 can potentially be amalgamated within the previous segment, thus accepting one slightly longer segment along the curve. If $L_2>\delta$, the nodes between the segments are adjusted to accommodate a slightly longer chord length $L_1+L_2/(N-1)$, where (N-1) is the number of segments. This does not yet guarantee that the length L_2' of the new left-over segment is zero, since distances in this procedure are measured along the chords, rather than along the curve. Iterations are therefore necessary.

   After segmentation, the straight lines connecting the end points of each segment form the first set of rods of the grid.

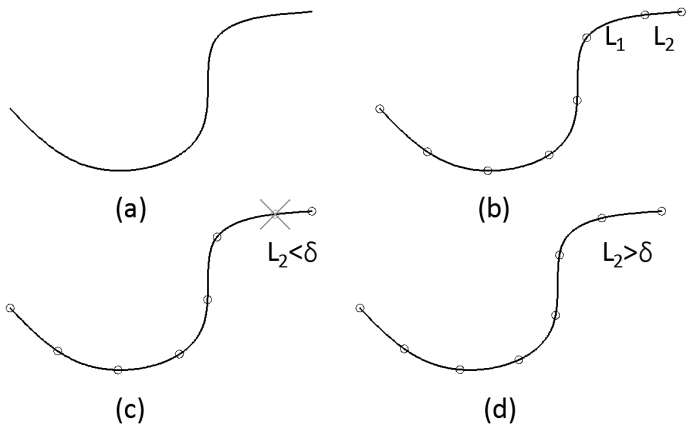

Fig.12. Segmentation of the curve: (a) Guideline; (b) First subdivision with chord length L_1; (c) Merging of the last two segments if $L_2 < \delta$, and (d) Iterative adjustment if $L_2 > \delta$.

8. The remaining rods of the grid are obtained by connecting points lying on adjacent curves (Fig.8 (f)). An algorithm was thereby used which makes a distinction between three sub-cases in order to reduce the possible occurrence of irregular grid cells containing very sharp angles and improve the grid quality. In order to automate this process, the following algorithm is followed:

First, the angles α and β determined by the i^{th} and the $(i+1)^{th}$ curve, as shown in Fig. 13, are calculated. Based on these angles, three different cases can be identified:

(a) Both α and β are smaller than (or equal to) 90°.

(b) One of the angles (either α or β) is larger than 90° and the other one is smaller than (or equal to) 90°.

(c) Both α and β are larger than 90°.

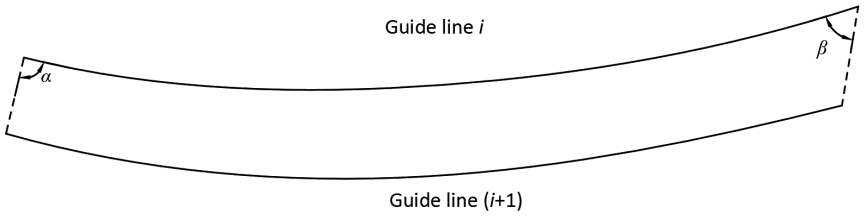

Fig.13. Angles between adjacent curves ($\beta \leq \alpha \leq 90°$).

All three cases lead to analogous procedures and the algorithm for case (a) can be adapted to the other two cases in an almost trivial way. Therefore, the discussion is here focused on the case (a).

As shown in Fig.14 (a), we consider two adjacent curves with n points ($\mathbf{P}_0$, $\mathbf{P}_1$, …, $\mathbf{P}_{n-1}$) on the i th curve and m points ($\mathbf{Q}_0$, $\mathbf{Q}_1$, …, $\mathbf{Q}_{m-1}$) on the (i+1)th curve. Indicating the angle at point B in the triangle ABC as $\angle$ABC, we successively calculate (Fig.14 (b)): $\angle Q_0P_1P_2$, $\angle Q_0P_2P_3$,… until we reach a point $\mathbf{P}_k$ where $\angle Q_0P_kP_{k+1} > 90°$. The point Q_0 is then connected to $\mathbf{P}_1$, $\mathbf{P}_2$ … $\mathbf{P}_k$ by straight lines (Fig.14 (b)). The above procedure is subsequently repeated for the next point $\mathbf{Q}_1$ (i.e. a point $\mathbf{P}_l$ is sought for which $\angle Q_1P_lP_{l+1} > 90°$), as well as for $\mathbf{Q}_2$, $\mathbf{Q}_3$, …. When either the point $\mathbf{Q}_{m-1}$ at the end of the (i+1)th curve is reached, or the point $\mathbf{P}_{n-1}$ at the end of the ith curve, three possible scenarios can be envisaged:

(a) There are unconnected points $\mathbf{P}_q$ … $\mathbf{P}_{n-1}$ left on the ith curve (Fig. 14(c)). In this case, those residual points are connected to $\mathbf{Q}_{m-1}$ (as shown with dashed lines in Fig. 14(c)).

(b) All points on both curves are connected and there are no residual points (Fig. 14(d)).

(c) There are residual points $\mathbf{Q}_q$ … $\mathbf{Q}_{m-1}$ on the (i+1)th curve (Fig. 14(e)). In this case, those residual points are connected to $\mathbf{P}_{n-1}$ (as shown with dashed lines).

It can be seen from Fig.14 that sharp angles may still exist in the resulting grid. However, some minor merging and deleting operations can be used to improve the grid.

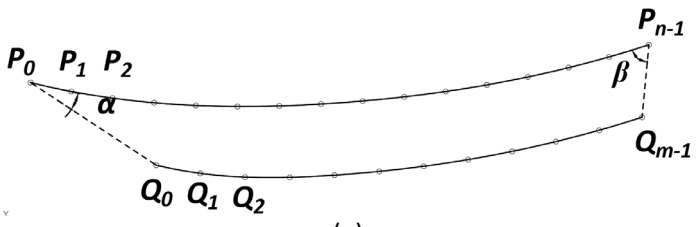

(a)

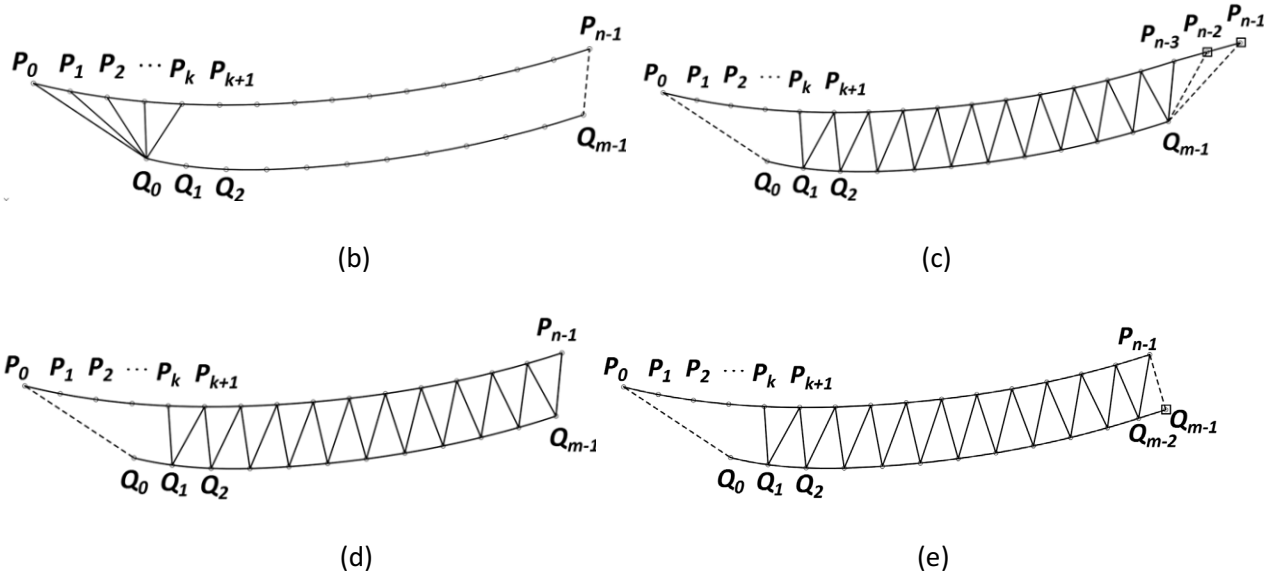

Fig.14. Connecting points on two adjacent guide lines.

5.2 Case Studies

5.2.1 Chen Shan Botanical Gardens

The Shanghai Chen Shan Botanical Gardens contain three conservatories with an irregular 'bean shape' in plan view (Fig. 15). As a case study, a grid was generated for one of the buildings using the GSM. An NURBS surface was first fitted to the shape, as shown in Fig. 16.

Fig. 15. Panorama of Chen Shan Botanical Gardens.

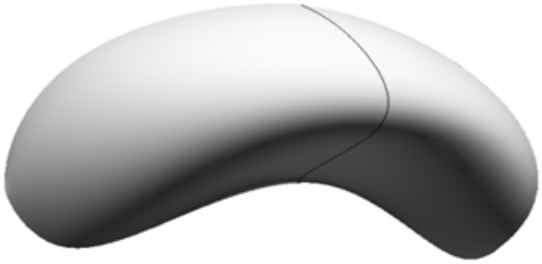

Fig. 16. NURBS surface and guide line.

The direction of the initial guide line had a substantial impact on the resulting grid. Three different initial guide lines were considered in this example, as shown in Fig. 16. In accordance with the GSM algorithm the guide lines were translated in space over a constant distance, which sets the method apart from the 2G2V method applied on the same structure in Section 6.2.1. Figs. 17 and 18 present the resulting curves covering the surface. The computing time on a typical desktop computer are shown in Table 1 for these 3 cases. It took around 2 minutes to achieve the set of curves. The computing time needed for triangulation was negligible compared to the time used for guide line advancement.

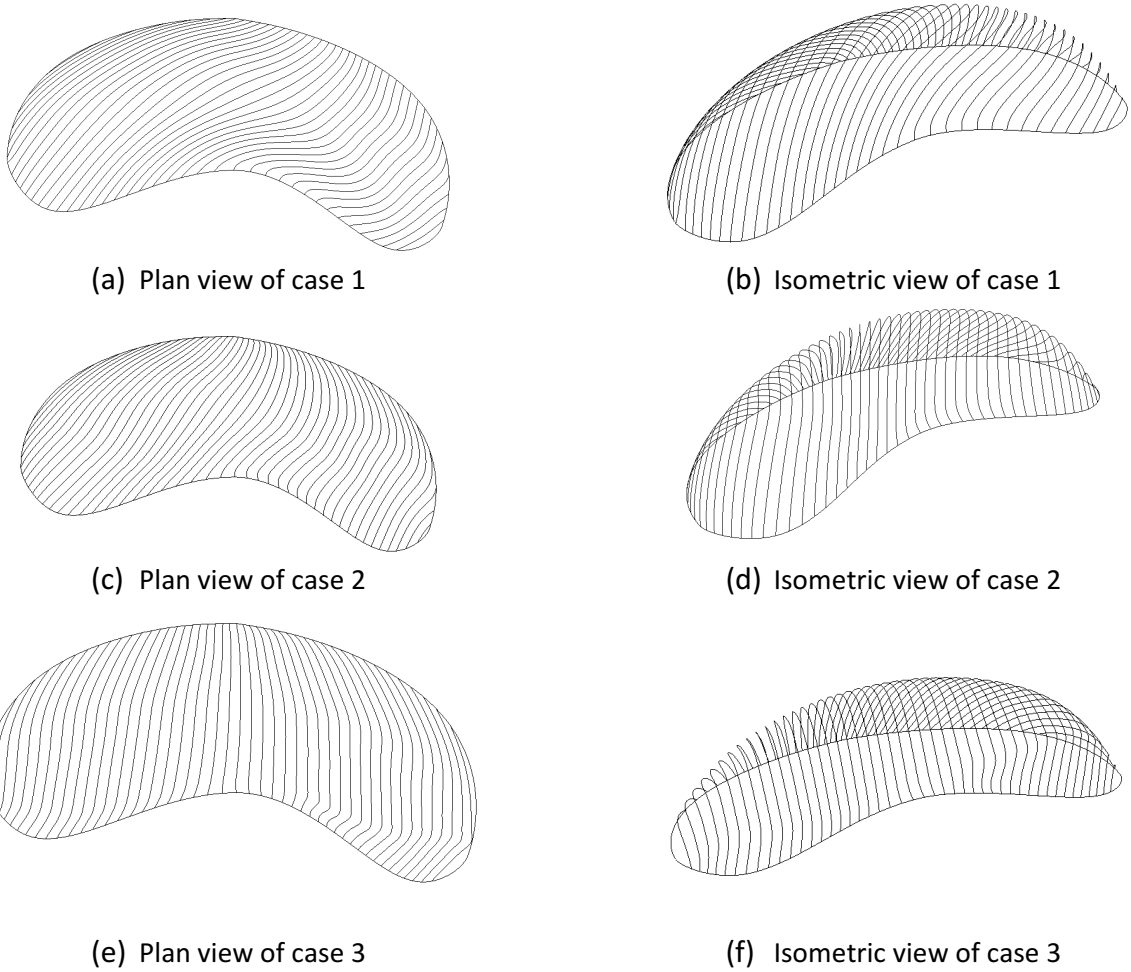

(a) Plan view of case 1 (b) Isometric view of case 1

(c) Plan view of case 2 (d) Isometric view of case 2

(e) Plan view of case 3 (f) Isometric view of case 3

Fig. 17. GSM results for Chen Shan Botanical Gardens with different initial guide lines

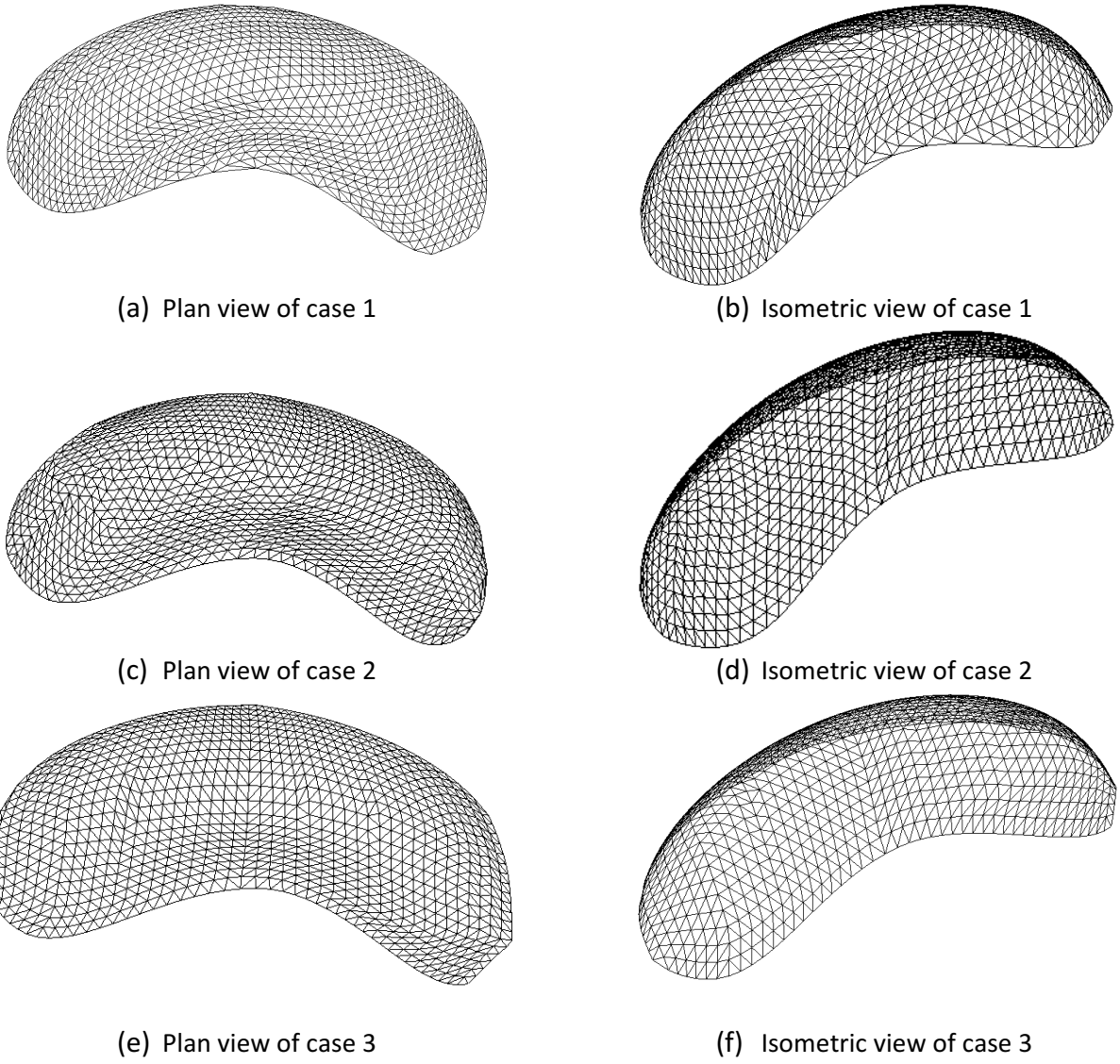

(a) Plan view of case 1 (b) Isometric view of case 1

(c) Plan view of case 2 (d) Isometric view of case 2

(e) Plan view of case 3 (f) Isometric view of case 3

Fig. 18. Triangular grid pattern obtained after connecting the adjacent guide lines shown in Fig.17

Table 1. Computing times for triangular grid generation for Chen Shan Botanical Gardens

Cases	Guide line generation computing time (ms)	Triangulation computing time (ms)	Total computing time (ms)
1 (Triangle)	78492	7	78499
2 (Triangle)	112701	7	112708
3 (Triangle)	115750	5	115755

By combining two of the sets of guide lines shown in Fig.17, the diamond grid patterns shown in Fig.19 can be obtained. These quadrangular grids generated by the GSM are smooth and

homogeneous, although some triangular cells of small and irregular size are present on the boundaries.

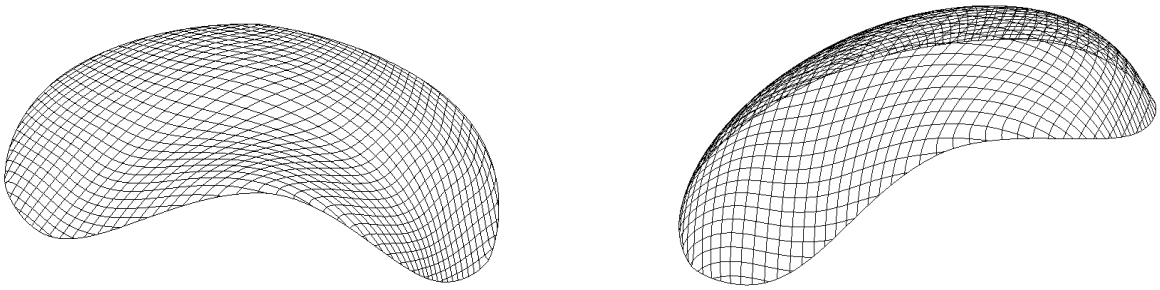

(a) Plan view (b) Isometric view

Fig.19. Quadrangular grid generated using the GSM for Chen Shan Botanical Gardens

In order to compare the generated grid to the results of the Mapping Method, a triangular grid was generated by adding diagonal rods in each quadrangular grid cell shown in Fig.19. The results are shown in Fig. 20, while the grid generated using the Mapping Method [24] is shown in Fig. 21.

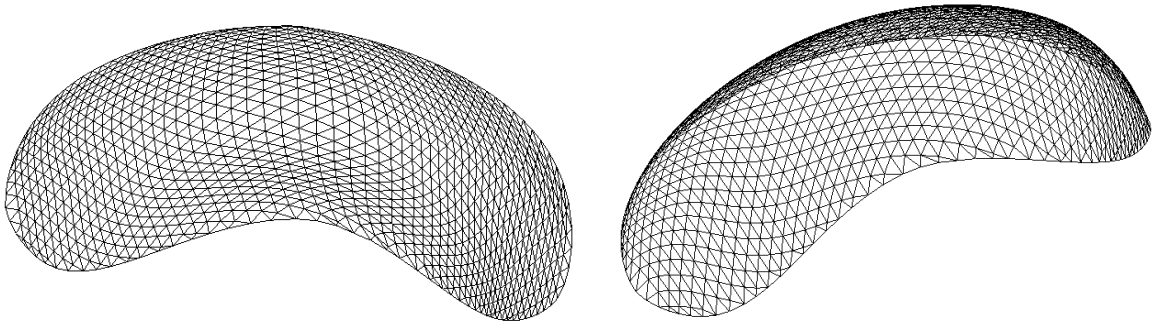

(a) Plan view (b) Isometric view

Fig. 20. Triangular grid pattern generated using the GSM for Chen Shan Botanical Gardens.

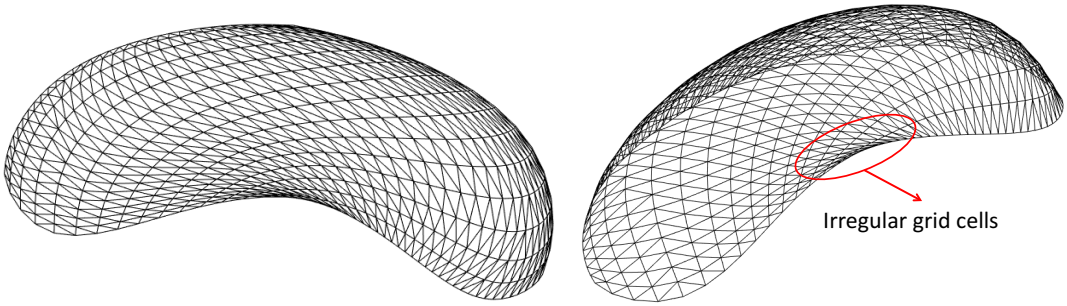

Fig.21. Grid pattern generated using the Mapping method [18] for Chen Shan Botanical Gardens.

A comparison between Figs.20 and 21 shows that, while fluent grids were obtained using both the GSM and the Mapping Method for the surface of the Chen Shan Botanical Gardens, the results of the Mapping Method prove to be visually smoother. However, the rod lengths obtained using the GSM are much more uniform than in the case of the Mapping Method. The latter method results in zones on the surface with grid cells which differ significantly in both size and shape from the rest of the surface. Moreover, fairly sharp corners are routinely encountered in the grid cells.

5.2.2 Extruded surface

In order to further test the algorithm, an arbitrary NURBS surface was generated, as shown in Fig.22. This surface was obtained by extruding a profile NURBS curve along a straight line segment while simultaneously scaling it. It is worth noting that this surface technically does not qualify as a free-form surface in its true sense. The left boundary was in this case chosen as an initial guide line. The GSM as well as the Mapping Method were applied, resulting in the grids shown in Fig.23 and 24, respectively. It can be concluded in this case that using the GSM and the Mapping Method both result in a grid pattern with great fluency and excellent uniformity of the rod lengths.

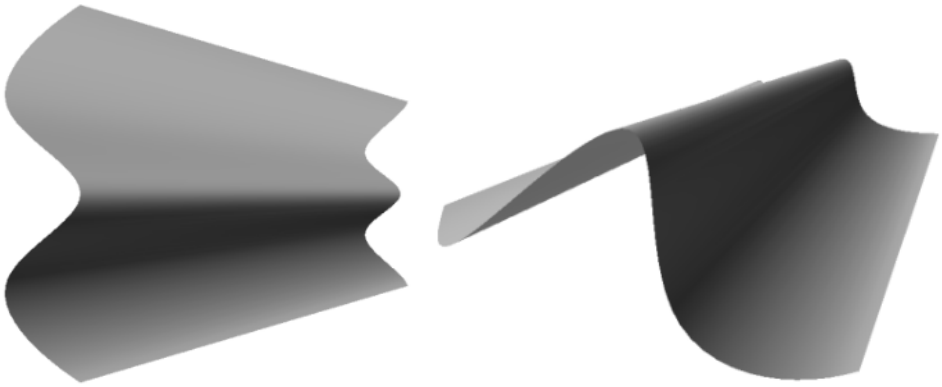

(a) Plan View (b) Isometric view

Fig. 22. Random surface.

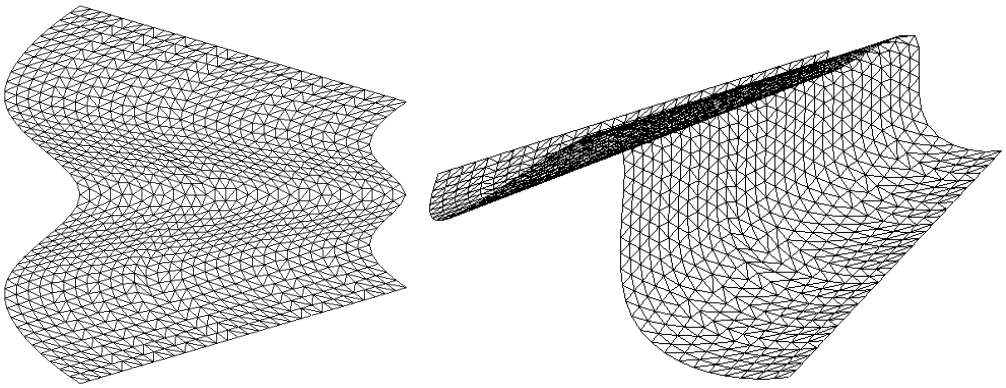

(a) Top View (b) Isometric view

Fig. 23. Resulting grid after application of GSM.

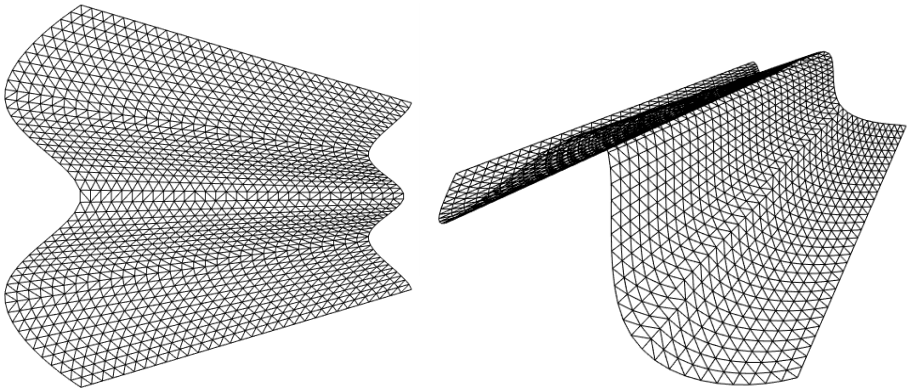

(a) Top View (b) Isometric view

Fig. 24. Resulting grid using the Mapping Method.

6 Two Guide Lines with Two End Vertices Method (2G2VM)

6.1 Algorithm Description

In contrast to the GSM, the 2G2VM requires the definition of not one, but two initial guide lines. Each of the guide lines intersects at its ends with the surface boundaries. These boundaries are subsequently subdivided into a number of equal (chord) length intervals separated by ‘vertices’. The original guide line is then advanced by moving the end points to the next two vertices on the boundaries while applying steps 4-6 of the previous section. The process is repeated for the remaining vertices. An identical procedure is then applied to the second guide line. The points of intersection of both sets of guide lines then form the nodes of the grid.

The main steps of the 2G2VM are shown schematically for a pair of red and blue guide lines in Fig. 25.

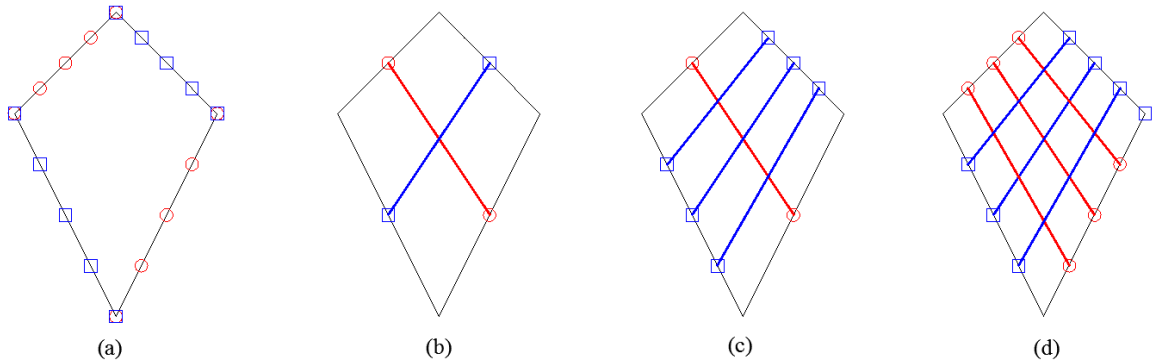

Fig.25. Main steps of the 2G2VM, shown schematically for a flat surface: (a,b) Two initial guide lines are defined and boundaries are divided; (c) New curves are generated by advancing the first guide line; (d) Second guide line is advanced to generate a grid.

It worth noting that, in many cases, no twin vertex exists for some of the vertices at one end of the boundary line, as shown in Fig.26. To solve this problem, the boundary curves should be extended. Several methods can be proposed to achieve this. For instance, a circle with a curvature equal to the curvature of the boundary curve at its end point can be used.

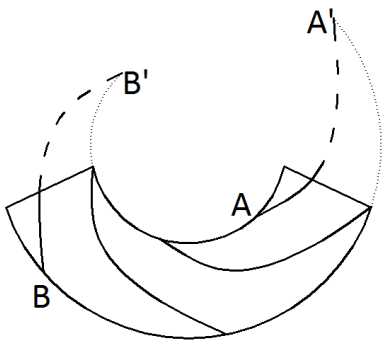

Fig. 26. Schematic diagram of curves after complementing the vertices A and B.

6.2 Case Studies

6.2.1 Chen Shan Botanical Gardens

The project of the Chen Shan Botanical Gardens previously discussed in Section 5.2.1 is again considered, this time using the 2G2VM, in order to allow a comparison with the GSM. The

boundaries of the surface were divided in 48 segments with equal chord length. The resulting curves, taking the same three initial guide lines defined in Section 5.2.1 as a starting point, are shown in Fig.27. The computing times on the same desktop computer are shown in Table 2 for the three cases. It took approximately 2 minutes to generate a set of curves. Both the GSM and the 2G2VM were able to generate sets of smooth curves, while the GSM curves appeared more uniform in terms of intermediate spacing.

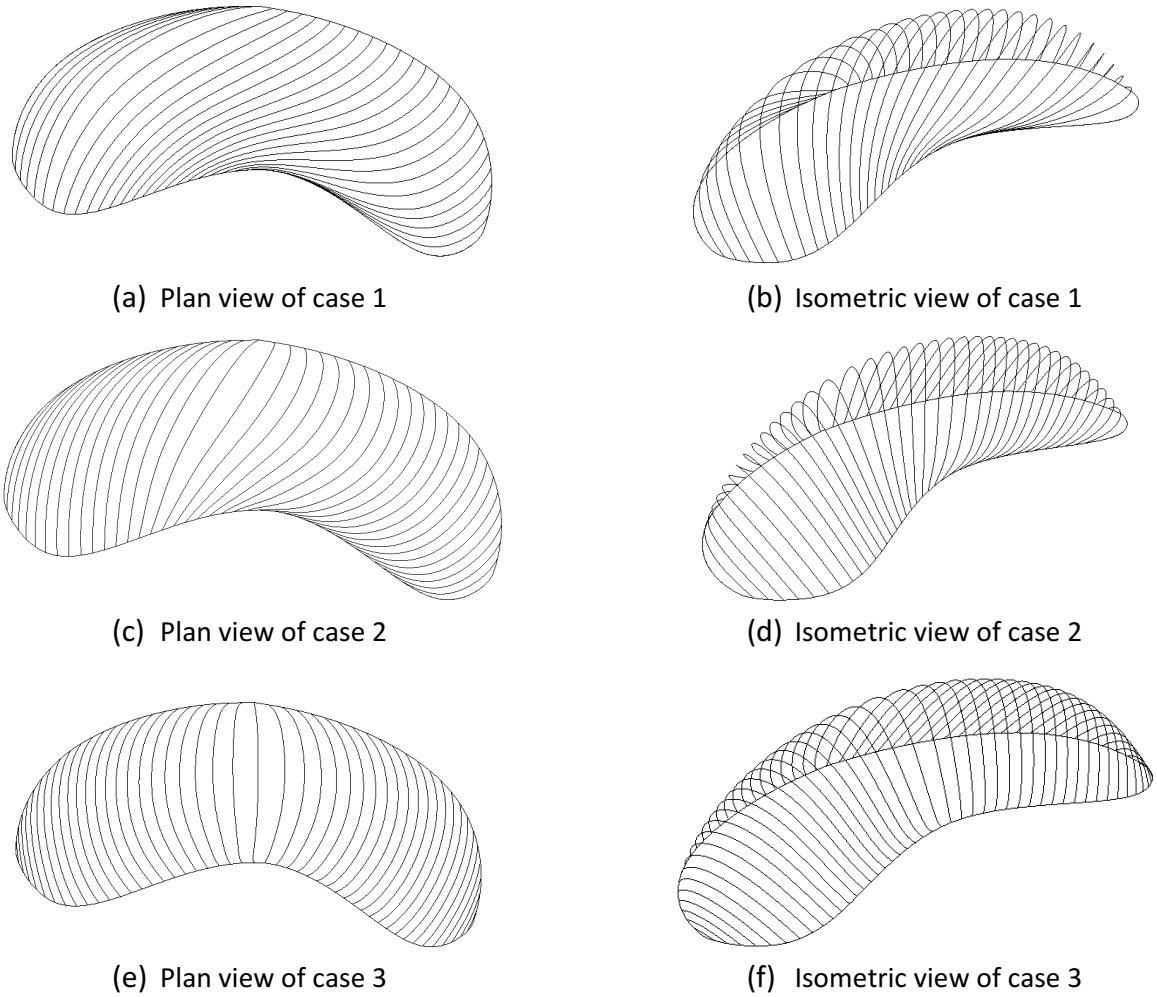

(a) Plan view of case 1 (b) Isometric view of case 1

(c) Plan view of case 2 (d) Isometric view of case 2

(e) Plan view of case 3 (f) Isometric view of case 3

Fig. 27. 2G2VM results for Chen Shan Botanical Gardens with different initial guide lines

Table 2. Computing time needed to generate guide line set using 2G2VM for Chen Shan Botanical Gardens

Cases	Computing time (ms)
1	102000
2	120000
3	117000

Combining two sets of curves from Fig. 27, the quadrangular grid shown in Fig.28 was obtained. Compared to the GSM results presented in Section 5.2.1 (Fig. 19), the grids are smoother and more fluent, although the cell size has become less homogeneous. There are also fewer irregular cells presenting near the boundary.

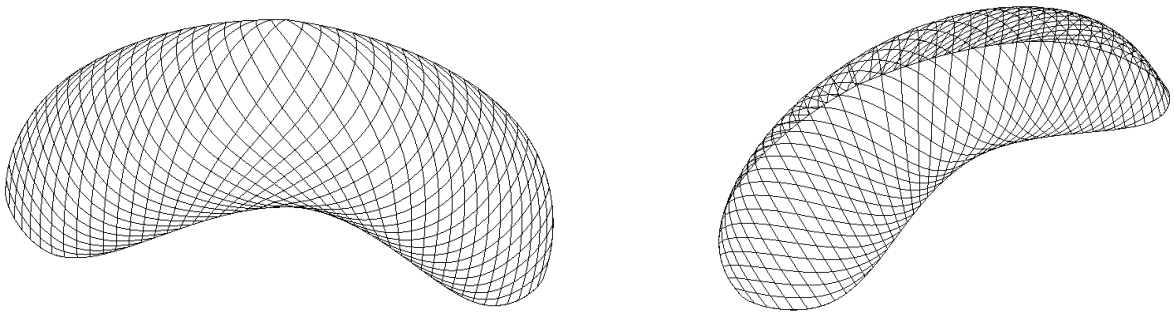

(a) Plan view (b) Isometric view

Fig. 28. Quadrangular grid pattern generated using the 2G2VM for Chen Shan Botanical Gardens

6.2.2 Sun Valley and Shenzhen Bay Sports Center

Sun Valley, located in the Shanghai World Expo Park, is made up of six single-layer steel lattice shells with circular or elliptical cross-sections in the horizontal plane. One of the shells is shown in Fig.29 (a). The height of the structure is 41.5 m and the diameters of the top and the bottom circles are 90 m and 20 m, respectively. This relatively simple structure is used to illustrate the methodology and efficiency of the proposed 2G2VM grid generation procedure. As shown in Fig.29 (b), an NURBS curved surface was first established to represent half of the shell. Two scenarios were investigated: two crossing oblique guide lines and two crossing boundary guide lines. The resulting grid patterns were also compared with one generated using the Mapping Method.

Fig. 29. Sun Valley in Shanghai World Expo Park: (a) perspective view and (b) NURBS surface.

Two Crossing Oblique Guide Lines

In this example, a grid pattern was generated using the 2G2VM which is similar to the "Big Tree" structure of Shenzhen Bay Sports Center (Fig.30 (a)). Two crossing oblique guide lines (as shown in Fig.30 (b)) were defined on the surface in order to achieve a rhomboid grid cell.

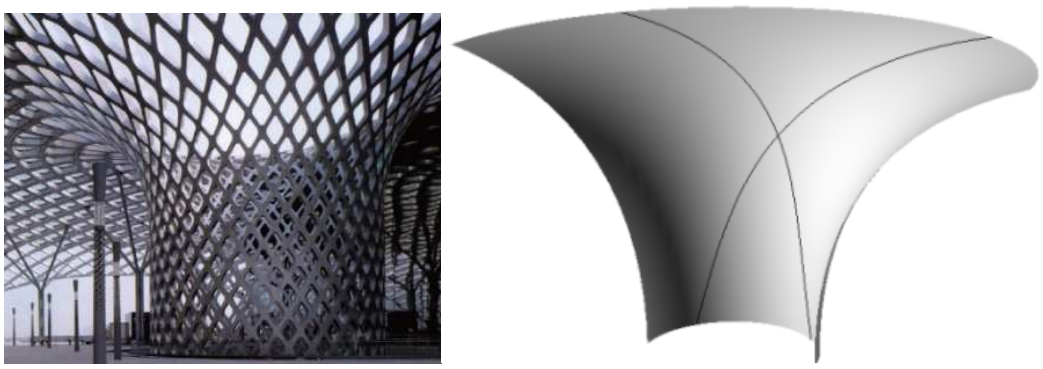

Fig.30. (a) "Big Tree" grid of Shenzhen Bay Sports Center (b) Two crossing guide lines.

Subsequently, pairs of vertices were formed by dividing the upper and lower semi-circles into 16 equal segments. Due to the fact that only half of the shell was modelled and that corresponding vertices were offset in the horizontal direction, the boundary curves had to be extended and additional vertices generated. This is illustrated in Fig.31. It is noted that, in this case, both guide lines made use of the same boundaries.

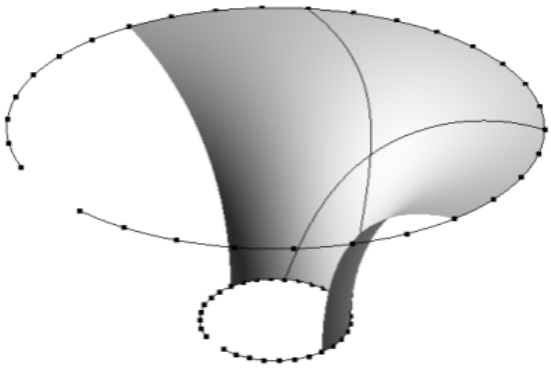

Fig. 31. Generation of vertex pairs.

The method results in a rhomboid grid by advancing the two guide lines, as shown in Fig. 32. Optionally, by materializing one of the diagonals of each rhomboid cell, a triangular grid pattern can be formed, as shown in Fig. 33.

For comparison, the Mapping Method was also used to generate quadrilateral and triangular grids and the results are shown in Fig.34. Both the 2G2VM and the Mapping Method resulted in satisfactory grid patterns. However, the 2G2VM achieved more fluency, while the designer, through the definition of the initial guidelines, also has more control over the grid in this method.

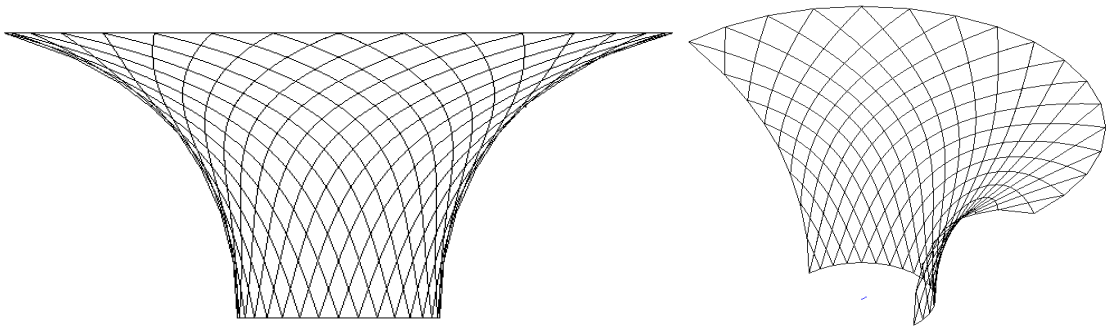

(a) Front View (b) Top View

Fig. 32. Quadrilateral mesh with two crossing oblique guide lines.

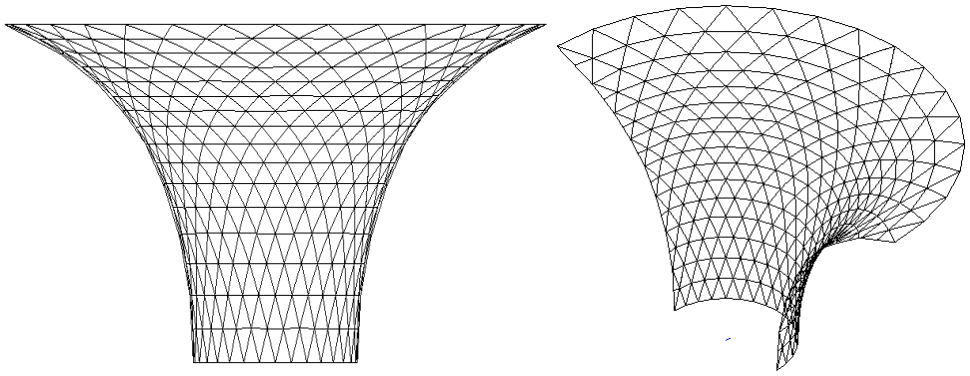

(a)Front view (b) Isometric view

Fig. 33. Triangular mesh with two crossing oblique guide lines.

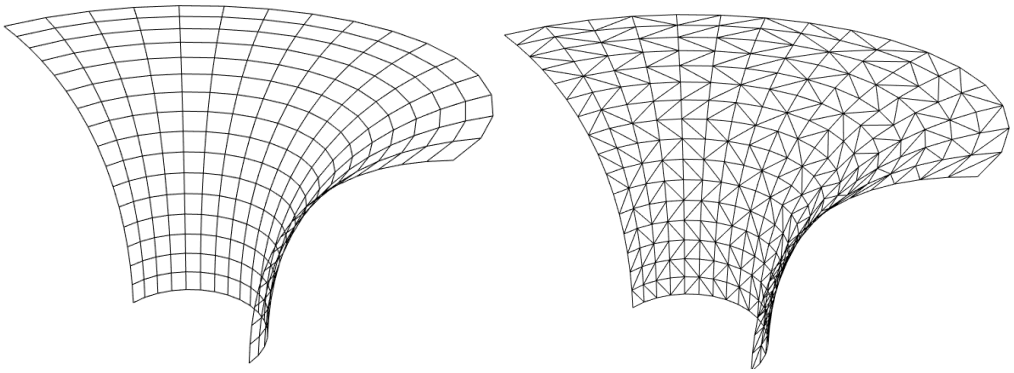

Fig. 34. Quadrilateral and triangular meshes using the Mapping method.

Two Crossing Boundary Guide Lines

In this example, the top semi-circle and the left side boundary were selected as guide lines, as shown in Fig. 35. Vertices were generated by dividing all four boundaries into 16 equal parts. By adopting the 2G2VM, a quadrilateral mesh was generated, as shown in Fig. 36. A triangular mesh (shown in Fig. 37) can also be obtained by making one of the diagonals of each quadrilateral grid cell explicit. The quadrilateral mesh is essentially identical to the one obtained using the Mapping Method (Fig. 34), while the 2G2VM achieves a more fluent triangular mesh thanks to avoiding the seemingly random orientation of the diagonals in the Mapping Method (Fig. 34).

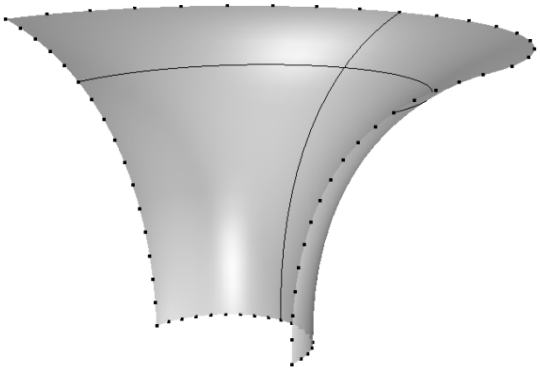

Fig. 35. Vertices on the boundary curves.

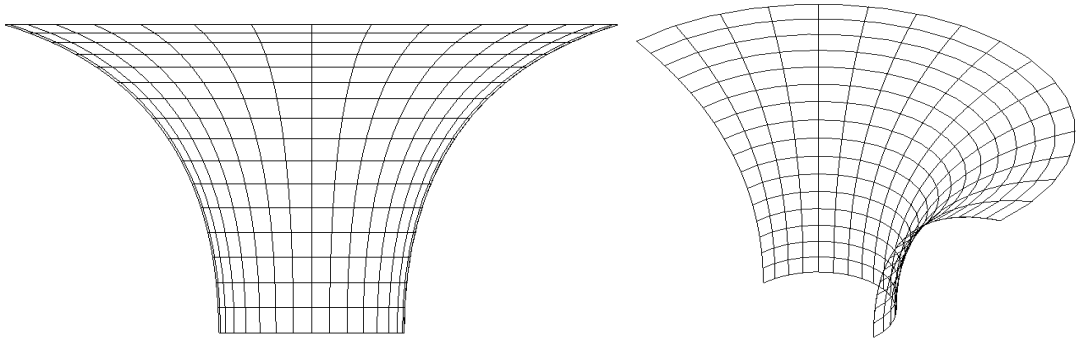

(a) Front view (b) Isometric view

Fig. 36. Quadrilateral mesh with two crossing boundary guide lines.

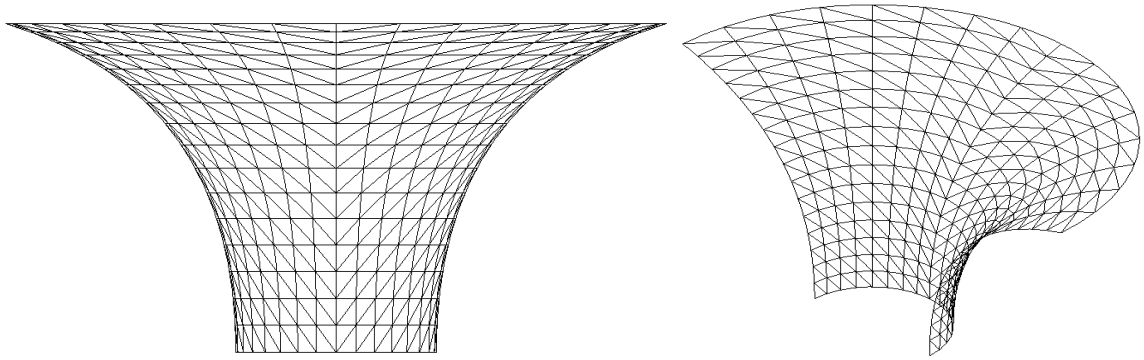

(a) Front view (b) Isometric view

Fig. 37. Triangular mesh with two crossing boundary guide lines.

It is noted that the resulting grids presented for the relatively simple case of the Sun Valley and Shenzhen Bay Sports Center can also be achieved in a more direct way by exploiting the symmetry of revolution i.e. by first discretizing the upper and lower boundary curves and then directly

connecting the opposite points. However, this example mainly serves to illustrate the methodology. In the next section, both the GSM and 2G2VM are applied to a more complex surface.

7 British Museum Great Court Roof

The steel and glass roof of the British Museum Great Court covers a rectangular area which is 70 m in width and 100 m in length. The Reading Room, which has a cylindrical shape with a diameter of 44 m, is located at the centre of the court. The shape of the roof can be expressed as a mathematical function and more information is provided in [25]. The rods in the roof range in length from 1 m to 3 m. As an additional case study the here proposed methods (GSM and 2G2VM) were applied to generate a grid on the roof of the British Museum Great Court. The original surface and mesh are shown in Figs. 38 (a) and (b), respectively.

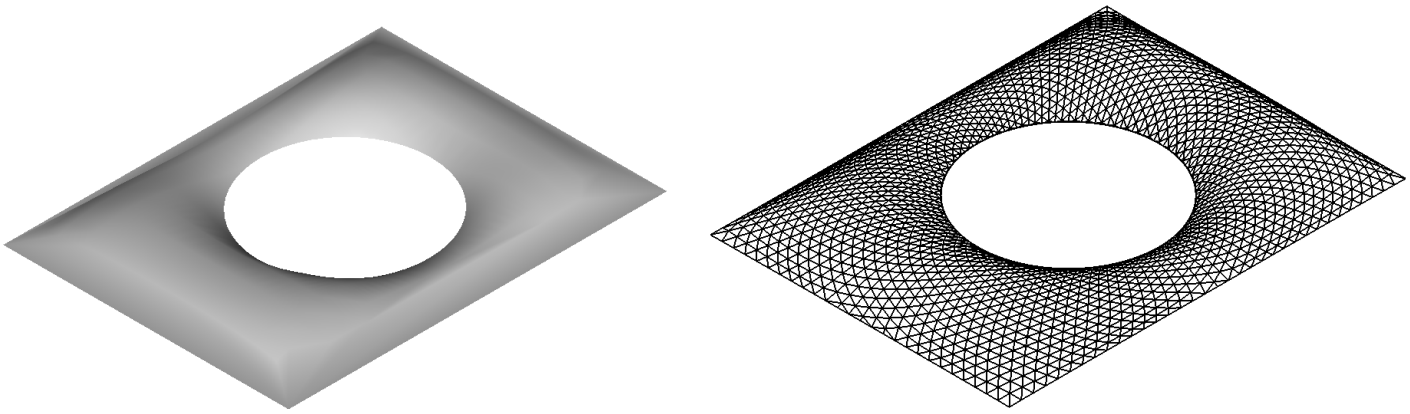

(a) original surface (b) original mesh

Fig. 38. The British Museum Great Court roof.

The surface was first divided into four sub-surfaces using the diagonals of the rectangular plan. Each method was then applied to the sub-surfaces, after which the grids of the sub-surfaces were merged together. Some of the intermediate steps, as well as the final grid resulting from the GSM are shown in Figs. 39 and 40, respectively. Figs. 41 and 42 illustrate the intermediate and final results using the 2G2VM.

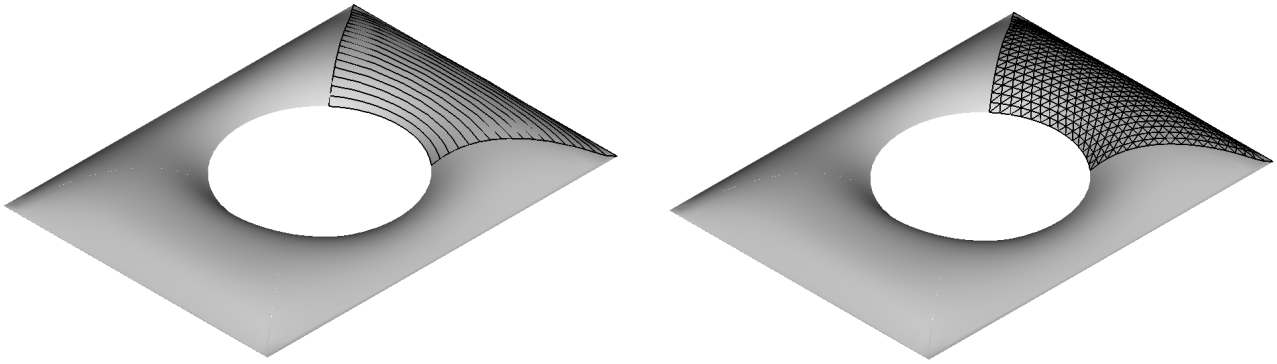

(a) Advancing the guide line on the sub-surface (b) Segmentation and connection

Fig. 39. Intermediate steps of grid generation using the GSM on the British Museum Great Court roof.

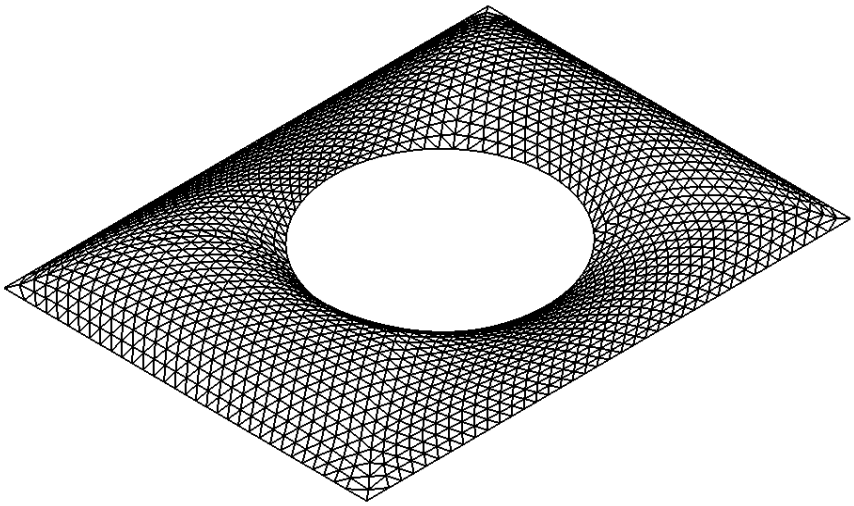

1

2 **Fig. 40.** Triangular grid on the British Museum Great Court roof using the GSM.

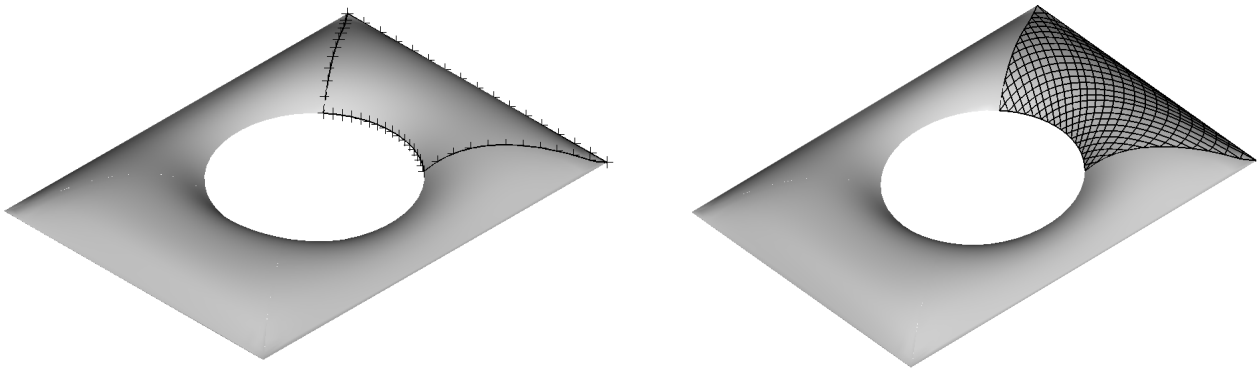

(a) Subdivision of the boundaries (b) Advancing the guide lines

Fig. 41. Intermediate steps of grid generation using the 2G2VM on the British Museum Great Court roof.

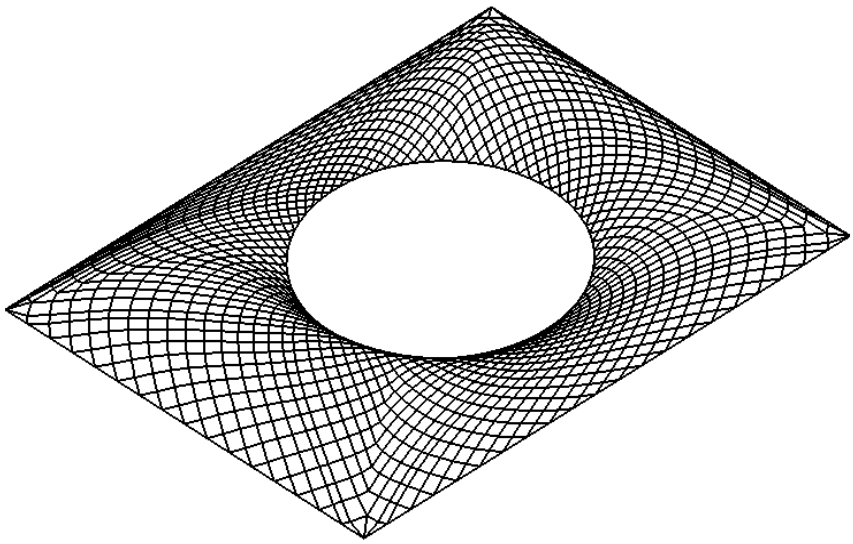

Fig. 42. Quadrilateral grid on the British Museum Great Court roof using the 2G2VM

The triangular grid pattern on the British Museum Great Court roof surface obtained using the GSM, pictured in Fig. 40, has somewhat similar features to the original design and shows very good fluency, although some irregularly sized and shaped cells exists along the diagonals near the corners. However, the rod length is more uniform in the GSM grid, due to the fact that the algorithm was developed specifically with rod uniformity in mind. Fig. 42 illustrates the quadrilateral grid generated using the 2G2VM. The fluency of the pattern and the uniformity of the rods are both very good, although some irregular cells are encountered along the boundary lines of the sub-surfaces.

The mean value and the variance of the rod lengths were calculated for each of the three grid patterns and are compared in Table 3. While the mean values of the rod lengths are approximately the same, the variance of the rod lengths is reduced by 42% compared to the original grid when using the GSM. This again illustrates the advantage of the GSM in obtaining uniform grids. On the contrary, the quadrilateral grid generated using the 2G2VM is far less uniform than the original triangular grid.

Table 3. Mean value and variance of the rod lengths in three grids

Grid generation method	Mean value of rod lengths (mm)	Variance of rod lengths (mm^2)
Original Mesh (triangular)	2047	207150
GSM (triangular)	2032	120136
2G2VM (quadrangular)	2126	464820

8 Software Development

Both presented grid generation methodologies (GSM and 2G2VM) were programmed into software called 'ZD-Mesher', specifically developed by the authors for the purpose of free-form grid generation. The software was developed for a Microsoft Windows operating system, using C++ and the IDE of Microsoft Visual Studio 2013. The GUI framework was based on MFC (Microsoft Foundation Classes). A screenshot of the GUI is shown in Fig. 43.

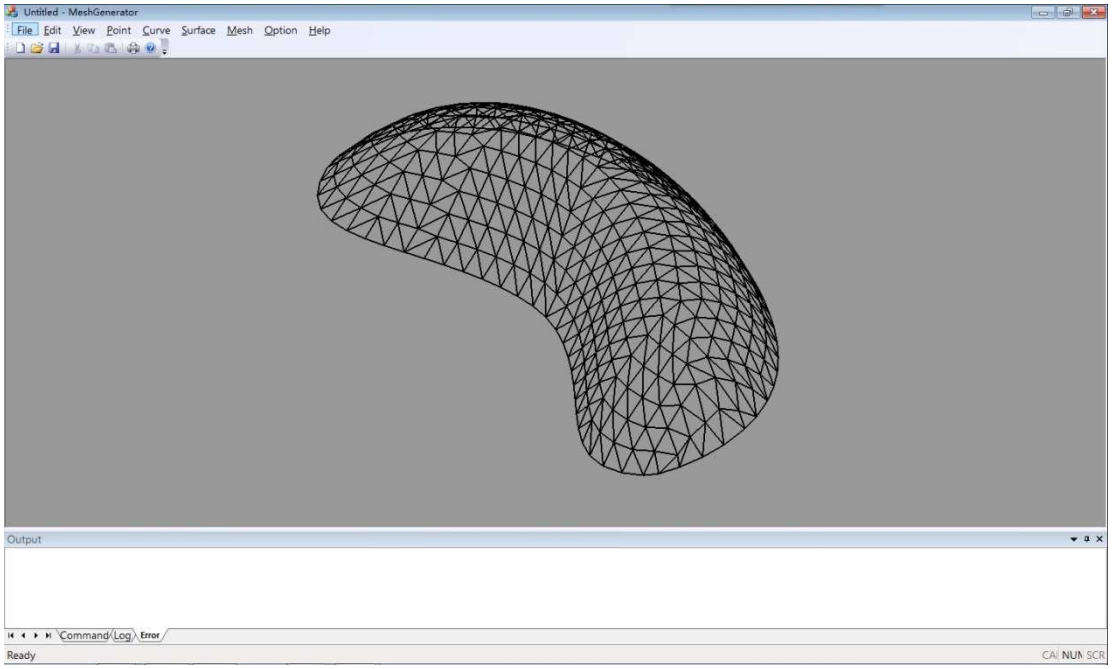

Fig. 43. GUI of the ZD-Mesher software.

The framework of the software is illustrated in Fig. 44. Apart from implementing the algorithms for grid generation, the software provides essential visualization and data exchange functions. It also provides commands assisting with sketching a curve on the surface, dividing a curve into

segments by number or by length and merging several curve sections into a single curve for further operations. The software is also able to exchange data with other commercial software packages as part of an integrated design process. Data formats such as IGES, STEP, BREP, and STL are supported. As a result, the software can communicate with almost any industrial CAD/CAM product. In addition, the software can export the geometric data to commercially available structural analysis packages such as ANSYS [27], ABAQUS [28] and SAP2000 [29].

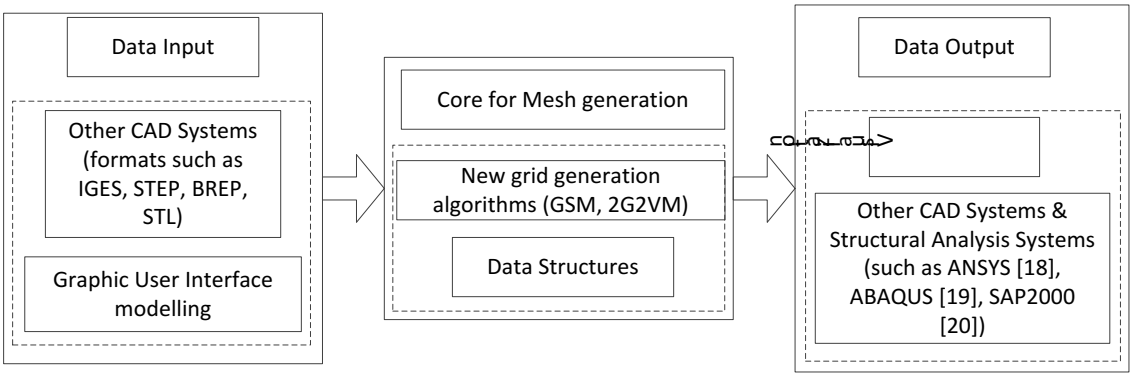

Fig. 44. Framework of the software.

9 Conclusions

The paper presents an efficient design tool for grid generation on a free-form surface. The proposed methods are based on the concept of a guide line, which allows an initial expression of architectural intent. The guide line is advanced over the surface by moving the endpoints, performing an affine transformation of the guide line and projecting it back onto the surface. Two variations are presented: the GSM, where a single guide line is used and the resulting curves are broken into segments, and the 2G2VM, where the grid is obtained as the intersection points of two sets of curves, each obtained by advancing a guide line. Consequently, the GSM yields triangular grids, while the 2G2VM results in quadrilateral grids (which optionally can be subdivided into a triangular grid).

Some practical case studies for both the GSM and 2G2VM are provided. The results indicate that a diverse range of constructible and visually expressive solutions can be obtained.

While the presented research has focused on developing a fast and straightforward approach which achieves grids with rods of balanced length, further research will aim to improve the algorithms by:

1) considering the planarity of the grid cells and other construction constraints in the grid generation process [30]. The planarity of quadrilateral grid cells is important when fastening the covering panels to the main structure in order to prevent possible brittle failure of materials due to warping.
2) giving the designer more freedom and flexibility by allowing the a variable advancing distance of the guide lines.

ACKNOWLEDGEMENT

The authors would like to express their gratitude to Dr. Paul Shepherd and Dr. Chris J K William at the University of Bath for their advice and for kindly providing the original surface and grid design of the British Museum Great Court roof.

This research was sponsored by the National Natural Science Foundation of China under Grant 51378457 and Grant 51678521 and by the Natural Science Foundation of Zhejiang Province under Grant LY15E080017. The authors would like to thank these funding schemes for their financial support.

REFERENCES

[1] Schlaich J, Schober H, Kürschner K. New Trade Fair in Milan–Grid Topology and Structural Behaviour of a Free-Formed Glass-Covered Surface. International Journal of Space Structures 2005;20:1-14.

[2] D'Amico B, Kermani A, Zhang H. Form finding and structural analysis of actively bent timber grid shells. Eng Struct 2014;81:195-207.

[3] Shepherd P, Richens P. The case for subdivision surfaces in building design. Journal of the International Association for Shell and Spatial Structures 2012;53:237-45.

[4] Ding H, Wang DW. Numerical simulation of wind loads and structural design optimization for the large span roof of Daishan Stadium. Proceedings of The 8th National Civil Engineering Forum for Graduate Students-NCEFGS 2010. Hang Zhou, China: Zhejiang University; 2010.
[5] D'Amico B, Kermani A, Zhang H, Pugnale A, Colabella S, Pone S. Timber gridshells: Numerical simulation, design and construction of a full scale structure. Structures: Elsevier; 2015. p. 227-35.
[6] Richardson JN, Adriaenssens S, Coelho RF, Bouillard P. Coupled form-finding and grid optimization approach for single layer grid shells. Eng Struct 2013;52:230-9.
[7] Oh J, Ju YK, Hwang K-J, Kim S-D, Lho S-H. FREE node for a single layer free-form envelope subjected to bending moment. Eng Struct 2016;106:25-35.
[8] D'Amico B, Kermani A, Zhang H, Shepherd P, Williams CJK. Optimization of cross-section of actively bent grid shells with strength and geometric compatibility constraints. Comput Struct 2015;154:163-76.
[9] Bouhaya L, Baverel O, Caron JF. Optimization of gridshell bar orientation using a simplified genetic approach. Struct Multidiscip O 2014;50:839-48.
[10] Cui CY, Jiang BS. A morphogenesis method for shape optimization of framed structures subject to spatial constraints. Eng Struct 2014;77:109-18.
[11] Park P, Gilbert M, Tyas A, Popovic-Larsen O. Potential use of structural layout optimization at the conceptual design stage. International Journal of Architectural Computing 2012;10:13-32.
[12] Shepherd P, Pearson W. Topology optimisation of algorithmically generated space frames. Proceedings of the IASS Symposium Wroclaw, Poland2013.
[13] Wu H, Ye J, Gao BQ, Shan YL, Zhang C. On the robustness of cable supported structures, a theoretical and experimental study. Journal of the International Association for Shell and Spatial Structures 2014;55:243-56.
[14] Winslow P, Pellegrino S, Sharma SB. Multi-objective optimization of free-form grid structures. Struct Multidiscip O 2010;40:257-69.
[15] Su L, Zhu SL, Xiao N, Gao BQ. An automatic grid generation approach over free-form surface for architectural design. J Cent South Univ 2014;21:2444-53.
[16] Liu Y, Xing HL, Guan ZQ. An indirect approach for automatic generation of quadrilateral meshes with arbitrary line constraints. International Journal for Numerical Methods in Engineering 2011;87:906-22.
[17] Du Peloux L, Baverel O, Caron J-F, Tayeb F. From shape to shell: a design tool to materialize freeform shapes using gridshell structures. Design Modelling Symposium Berlin2013.
[18] Hennicke J, Schaur E. IL 10 Gitterschalen–Grid Shells. Karl Krämer Verlag Stuttgart; 1975.
[19] Muylle J, Iványi P, Topping B. A new point creation scheme for uniform Delaunay triangulation. Eng Computation 2002;19:707-35.
[20] Branets L, Carey GF. A local cell quality metric and variational grid smoothing algorithm. Engineering with Computers 2005;21:19-28.
[21] Schiftner A, Balzer J. Statics-sensitive layout of planar quadrilateral meshes. Advances in Architectural Geometry 2010 2010:221-36.
[22] Piegl L, Tiller W. The NURBS book: Springer Science & Business Media; 2012.
[23] Piegl L. On NURBS: a survey. IEEE Computer Graphics and Applications 1991:55-71.
[24] Hannaby SA. A Mapping Method for Mesh Generation. Computers & Mathematics with Applications 1988;16:727-35.
[25] Williams CJ. The analytic and numerical definition of the geometry of the British Museum Great Court Roof. In: Mathematics & design 2001; Deakin University; 2001:434-40.
[26] De Berg M, Van Kreveld M, Overmars M, Schwarzkopf OC. Computational geometry: Springer; 2000.
[27] ANSYS. User's Guide, Release 14.5. Ansys Inc, Canonsburg 2012.
[28] ABAQUS 6.13. Analysis User's Guide, Dassault Systems 2013.
[29] Berkeley C. Computer program SAP2000 v14. 2.4. Computers and Structures Inc, Berkeley, California 2011.
[30] Adriaenssens S, Ney L, Bodarwe E, Williams C. Finding the form of an irregular meshed steel and glass shell based on construction constraints. Journal of Architectural Engineering 2012;18:206-13.